Closed-Loop System Identification of Cardiovascular Control Mechanisms in Diabetic Autonomic Neuropathy

by

Ramakrishna Mukkamala

Bachelor of Science in Engineering
Biomedical and Electrical Engineering
Duke University (1993)

Submitted to the Department of Electrical Engineering and Computer Science
in partial fulfillment of the requirements for the degree of

Master of Science

at the

Massachusetts Institute of Technology

May, 1995

Signature of Author _____
Department of Electrical Engineering and Computer Science
May 26, 1995

Certified by _____
Richard J. Cohen
Thesis Supervisor

Accepted by _____
Frederic R. Morgenthaler
Chairman, Department Committee on Graduate Studies

Closed-Loop System Identification of Cardiovascular Control Mechanisms in Diabetic Autonomic Neuropathy

by

Ramakrishna Mukkamala

Submitted to the Department of Electrical Engineering and Computer Science on May 26, 1995, in partial fulfillment of the requirements for the degree of Master of Science

Abstract

The primary focus of this thesis is on the presentation of a sensitive, quantitative method that requires minimal subject cooperation for the assessment of the autonomic nerve damage frequently associated with diabetes mellitus. The method employs a system identification procedure to estimate the open-loop couplings between the beat-to-beat fluctuations in heart rate, arterial blood pressure, and instantaneous lung volume described in a closed-loop model of short-term cardiovascular control mechanisms. This model contains four couplings, two (ILV→HR and BAROREFLEX) of which are considered autonomically mediated; one (ILV→ABP), mechanically mediated; and the other (CIRCULATORY MECHANICS), primarily mechanically mediated but also autonomically influenced. The model also includes two noise perturbations. These couplings are estimated with data collected non-invasively from both control subjects and subjects with diabetes mellitus. The subjects with diabetes mellitus are divided into three groups based on current accepted tests for the assessment of autonomic nervous function. The results show marked differences in ILV→HR and BAROREFLEX and minor differences in CIRCULATORY MECHANICS across the control and three diabetic groups. Just as important, there are no significant differences in ILV→ABP across these four groups. This study suggests that this closed-loop system identification procedure may provide a powerful tool for the assessment of autonomic neuropathy in patients with diabetes mellitus.

This thesis additionally presents a preliminary investigation on the nonlinear dynamics involved in short-term cardiovascular control mechanisms. In particular, a nonlinear system identification procedure is implemented to estimate the effects of the squared and cross product terms of arterial blood pressure and instantaneous lung volume on normal heart rate variability. The results indicate that these particular nonlinear terms do not play a significant role in the generation of heart rate variability.

Thesis Supervisor: Richard J. Cohen
Title: Professor, Harvard-MIT Division of Health Sciences and Technology

Acknowledgements

It gives me immense pleasure at this time to express my gratitude to Tom Mullen. Tom is a selfless person who is truly concerned with the well being of others, including myself. Not only did Tom help me get started in the Cohen lab, but he continued to offer me his support, advice, and time throughout the making of this thesis. Anytime I had a question or needed to discuss some research issue, Tom was always there. I learned so much from Tom during the many hours we spent in these discussion sessions. However, Tom did not just play the role of a research mentor, he also served as my "guidance counselor." If I had some sort of problem or concern, Tom was always willing to offer his experience and suggestions. I completely realize that Tom did not have to do all the things that he did for me and that is why I am so grateful. I am not sure if I will ever be able to help Tom the way he helped me, but maybe a situation will present itself in which someone else will need my time and attention. Knowing Tom, I am sure that is the way he would want it. Tom, you deserve all the best. Thanks, Tom. Tom, thanks.

I would also like to take this time to express my appreciation to the many others who contributed to this thesis. My thesis supervisor, Professor Richard Cohen introduced me to the field of system identification and its application to cardiovascular control systems. He gave me the freedom to balance research and coursework at my own discretion. Dr. Cohen also provided me with supplemental financial support on the spur of the moment that allowed me to attend MIT. Joanne Mathias, whom I have never had the privilege to meet, started this project and began the data analysis before I arrived at MIT. Dr. Roy Freeman reviewed Chapter 4 of this thesis, and he and Christopher Broadbridge provided the data used for this study. Derin Sherman generously reviewed this thesis and offered his comments. The rest of the Cohen lab members -Antonis Armoundas, Paul Belk, Yuri Chernyak, Ki Chon, Andy Feldman, Bin He, Yueh Lee, Moto Osaka, Thea Paneth, Simone Pola, and Tadashi Sasaki- also contributed to this thesis in one way or another. The Whitaker Foundation provided me with generous fellowship support during the creation of this thesis.

Finally, I would like to thank my parents, Durga and Mohanrao, and my sisters, Sasi and Chitra, for their constant support and encouragement during my many struggles at MIT.

Contents

List of Figures

List of Tables

Chapter 1

Introduction

Autonomic neuropathy is well recognized as a serious consequence of diabetes mellitus [15]. The clinical manifestations of diabetic autonomic neuropathy include postural hypotension, gastric symptoms, hypoglycemic unawareness, and sweating disturbances [13,15]. These clinical manifestations are slowly progressive, usually irreversible [13], and are associated with considerable mortality [17]. Consequently, it is essential to be able to quantify diabetic autonomic neuropathy so as to obtain a physiological measure of the progression of autonomic nerve damage and thus, guidance for treatment. As a result, standard autonomic tests based on cardiovascular reflexes to various physiological perturbations are commonly employed [19]. However, these tests are relatively insensitive, especially to early sympathetic nerve damage [16] and require the active cooperation of the subject, which may make the test results difficult to reproduce.

1.1 Objective

The primary objective of this thesis is to present a sensitive method that requires minimal subject cooperation for the assessment of autonomic nerve damage in subjects with diabetes mellitus. The method is based on employing a system identification

procedure to extract the information concerning cardiovascular control mechanisms inherent in the beat-to-beat fluctuations of cardiovascular variables. System identification involves the estimation of models of dynamic systems or couplings based on input and output data acquired from such couplings [28]. Therefore, system identification provides a means to examine the couplings of the beat-to-beat fluctuations in cardiovascular variables so as to quantitatively assess cardiovascular control mechanisms and consequently, autonomic nervous function. Specifically, a system identification procedure is implemented to estimate linear, time-invariant (LTI) mathematical models associated with a closed-loop model of short-term cardiovascular control relating the couplings between the beat-to-beat fluctuations in heart rate, arterial blood pressure, and instantaneous lung volume. This method is applied to data collected non-invasively from diabetic and control subjects to assess diabetic autonomic neuropathy.

Since nonlinear aspects of cardiovascular control mechanisms have been previously reported [29,42], an additional objective of this thesis is to present a preliminary analysis of the nonlinear dynamics involved in cardiovascular control. In particular, a nonlinear system identification procedure is implemented to estimate the effects of the squared and cross product terms of arterial blood pressure and instantaneous lung volume on normal heart rate variability.

1.2 Contents of Thesis

The contents of this thesis are organized in the following manner: Chapter 2 introduces the three components of this thesis, namely system identification, cardiovascular control mechanisms, and diabetic autonomic neuropathy. This chapter also discusses the application of system identification to the study of cardiovascular control mechanisms and highlights some of the previous relevant studies. Chapter 3 presents a treatment of the closed-loop system identification procedure employed in this thesis in the context of a general system identification procedure presented in Chapter 2. Chapter 4 presents the application of the closed-loop system identification procedure

described in Chapter 3 to the study of diabetic autonomic neuropathy. Chapter 5 presents a preliminary study of the nonlinear dynamics involved in cardiovascular control mechanisms, particularly in the generation of normal HR variability.

Chapter 2

Background

This chapter provides background information on the three components of this thesis, namely system identification, cardiovascular control mechanisms, and diabetic autonomic neuropathy. The chapter also includes a section about some aspects of the application of system identification to the study of cardiovascular control mechanisms, including highlights of previous relevant studies.

2.1 System Identification

This section provides an introduction to system identification by summarizing material in [5,24,28,39]. System identification is the field of estimating models of dynamic systems based on the observed input and output data from such systems. Science also involves developing models (such as laws and hypotheses) based on observations and so, system identification, in broadest terms, is integral to the scientific method. The applicability of system identification is virtually unlimited as dynamic systems are prevalent everywhere in this world.

2.1.1 Dynamic Systems

The notion of a dynamic system is illustrated in Figure 2-1. The system is driven by external stimuli $u(t)$ and $v(t)$ to produce an observable quantity $y(t)$ with t denoting time. The observer can control and measure $u(t)$ but not $v(t)$. Therefore, $u(t)$ is called the input, while $v(t)$ is referred to as a disturbance. The observable quantity $y(t)$ is called the output. For causal, dynamic systems, the present output value not only depends on the present value of the external stimuli but on their past values as well. Some examples of dynamic systems are aircrafts, robots, and as pertaining to this thesis, cardiovascular control mechanisms.

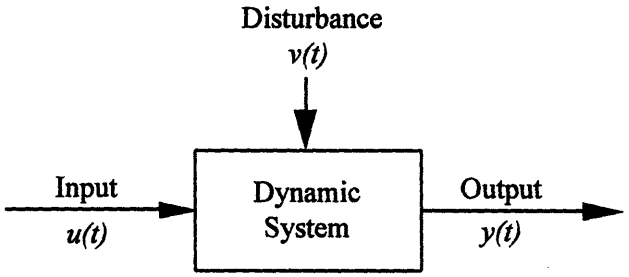

Figure 2-1: The notion of a dynamic system.

2.1.2 Modeling Dynamic Systems

The need for modeling dynamic systems often stems from the design problem. For example, in order to design a regulator for a particular system, some model of the interactions of the inputs, disturbances, and output of that system is necessary. However, design is not the only aim of system identification. System identification is also motivated by the need to obtain an understanding of the system itself. This is the motivation for system identification in this thesis. Several types of models can be used to describe dynamic systems. These include mental models, nonparametric models, and parametric models. A mental model does not involve any mathematical formulation. An example of a mental model is the knowledge that pushing the brake of a car decreases the

speed of the car. A nonparametric model is described by a graph or a table and can involve mathematical formulation. An example of a nonparametric model without mathematical formulation is a step response that is constructed by simply exciting the system with a unit step and measuring the resulting output. An example of a nonparametric model with mathematical formulation is the optimal transfer function in the least squares sense computed via FFT-based spectral analysis. This type of nonparametric model will be encountered again in Section 2.4.3. Parametric models typically involve mathematical formulations with adjustable parameters. The most common examples of parametric models are difference or differential equations. It should be noted that transfer functions can also be constructed from the parameters of such equations; however, in this case, the transfer functions are considered to be parametric. In this thesis, parametric models in the form of difference equations are employed.

System identification is one of two approaches for modeling dynamic systems. The other approach is mathematical modeling and is based on applying physical laws, such as Ohm's Law and Kirchhoff's Laws, to describe the dynamic nature of a system. Although mathematical modeling seems more desirable, it turns out that system identification is often more useful. In many cases, the system to be modeled is either too complex to be formulated on the basis of first principles or little if any *a priori* information is known about the system. In fact, the historical motivation of system identification was to design control strategies for such systems. Additionally, many models based on physical insight often contain parameters that are unknown. In these cases, system identification can be applied to identify the unknown parameters.

2.1.3 System Identification Procedure

The estimation of models from experimental data typically involves the following four steps:

1) *Generation of input-output data.* This step includes experiment design and data collection and processing. Experiment design deals with such issues as what signals to measure, when to measure them, and whether these signals are related in open- or closed-loop. The goal of experiment design is to obtain data that is maximally informative

subject to any existing constraints. This is equivalent to the inputs being *persistently exciting* which roughly means that all modes of the system are being excited by the inputs. The mathematical details of persistently exciting inputs will be discussed in Section 3.4.2. However, in some situations, the observer may not be able to control the inputs and must consequently use data from the normal operating conditions of the system. Data collection and processing deals with the measurements and signal processing involved in the generation of the input-output data. The objective of data collection and processing is to provide the most cleanest data possible. Clearly, good models can only result from good data.

2) *Selection of a candidate set of models.* This step is often the most difficult in the system identification procedure. In some cases, the system can be mathematically modeled with unknown parameters and consequently, a candidate set of models can be chosen accordingly. In other cases, the system is too complex or little is known about the system, and models must be chosen without regard to physical insight. This is often referred to as a black box approach. The first step in this approach involves choosing the type of model, generally a choice between nonparametric and parametric models. Since parametric models are employed in this thesis, the remainder of this procedure will be based on such models. As mentioned previously, parametric models are commonly difference or differential equations that have adjustable parameters. Generally, in the next step of the black box approach, a candidate set of parametric models is selected by choosing first a particular form of a difference or differential equation and then a set of different parameterizations for that equation. A parameterization is defined to be the collection of all the adjustable parameters in a difference or differential equation.

3) *Determination of the "best" model in the set.* This step first deals with determining the "best" parameterization from the input-output data and the set of parameterizations based on some criterion. The "best" parameterization is generally determined with one of the available information criterion tests such as the Rissanen's minimum description length (MDL) criterion or Akaike's Final Prediction Error (FPE). These tests find the proper balance between the number of parameters in a model and the loss function (some function of the difference between the actual output and the output produced by the

model). A model with too many parameters will produce a small loss function but at the same time it will model the noise. This is referred to as overparameterization. A model with too few parameters or underparameterization will produce a larger loss function which essentially means that the model does not explain the dynamics of the system. Therefore, information criterion tests essentially penalize the loss function by the number of parameters that comprise the model. Once the "best" parameterization is chosen, the "best" parameters can be estimated from the input-output data based on an identification method such as least squares. The identification methods are usually based on a minimization of the loss function. Clearly, an important requirement of an identification method is that the estimated parameters approach their true value as the data length approaches infinity. If this is the case, the system is rendered *identifiable*. It should be noted that transfer relations can also be computed from the estimated parameters. This often provides additional intuition about the estimated model.

4) *Validation of the "best" model.* This step deals with the question of whether the "best" model in the set provides an appropriate representation of the system. One way to deal with this question is to verify that the model describes the true system. Since the true system is not known, this amounts to confirming that the model is reasonable based on any *a priori* information. Another way to deal with this question is to determine if it is likely that the actual data was generated from the model. This can often be determined by testing the whiteness of the residual error (difference between the actual output and the output produced by the model) as some identification methods such as least squares require this feature. Perhaps the best way to deal with this question is to generate new input-output data from the system and see if the same model results. (Unfortunately, this validation method is not employed in this thesis, because the data records are not long enough.) Note that this step renders system identification to be an iterative procedure. If the model is not validated, then steps 1, 2, and/or 3 should be adjusted and the procedure should be repeated again until the "best" model is validated. Figure 2-2 shows a flowchart for the general system identification procedure.

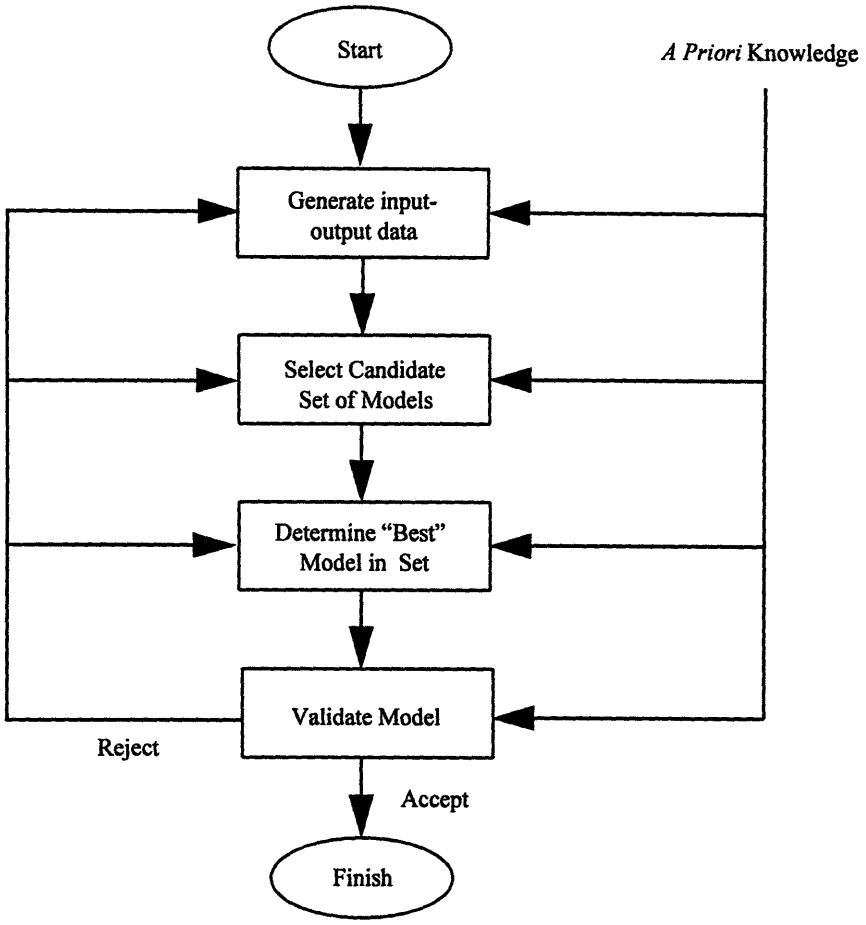

Figure 2-2: A flowchart of the system identification procedure. Modifed from [39].

2.2 Cardiovascular Control Mechanisms

This section presents some of the basic concepts of the short-term control mechanisms of the cardiovascular system by summarizing material from [8,14,22,23]. The cardiovascular system which consists of the heart and blood vessels is a transport system for blood. This transport system makes it possible for nutrients, gases, waste products, hormones, and fluids in blood to be exchanged between different tissues of the body. The required flow of blood to the tissues of the body vary since the metabolic

needs of each tissue differ. Therefore, each individual tissue can control its own local blood flow. This is referred to as the intrinsic control of the cardiovascular system.

The flow of blood from the heart to the vascular beds of the many tissues can be conceptualized with the electrical circuit in Figure 2-3. This circuit illustrates that the heart and the vascular beds can be respectively thought of as a current source and resistances connected in parallel. Note that the electrical variables of the circuit are represented with their analogous cardiovascular variables. The rate of blood flow f_i through the i^{th} vascular bed is as follows:

$$f_i = \frac{P_a - P_f}{R_i}$$

where P_a is arterial pressure, P_f is the filling pressure, and R_i represents the vascular resistance of the i^{th} vascular bed. Since arterial pressure is generally much greater than the filling pressure, the following approximation can be made:

$$f_i \approx \frac{P_a}{R_i}.$$

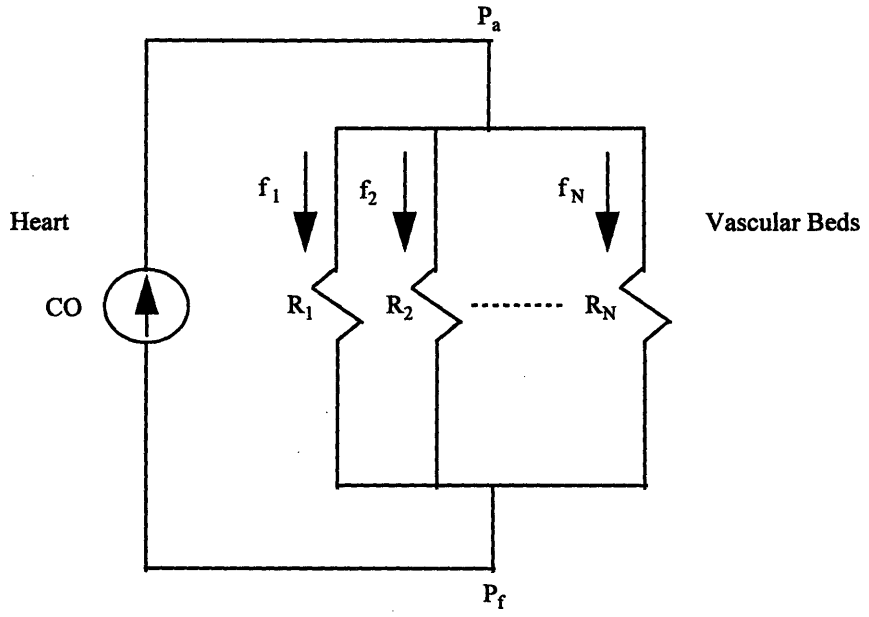

Figure 2-3: Electrical circuit model relating cardiac output (CO), arterial pressure (P_a), filling pressure (P_f), local vascular resistance (R_i), and local blood flow (f_i). Modified from [14].

Since adjustments in arterial pressure will influence blood flow to all vascular beds, the local control of blood flow must be achieved by adjusting local vascular resistance. Consequently, it is of paramount importance that arterial blood pressure remain constant or nearly constant. Otherwise, with varying arterial blood pressure, it would never be known whether adjustments in resistance would result in the appropriate changes in local blood flow. Therefore, the cardiovascular system includes a complex regulatory system that maintains arterial blood pressure within narrow limits. This is referred to as the extrinsic control of the cardiovascular system and is the focus of this thesis. It should be noted that the term cardiovascular control will henceforth refer specifically to extrinsic cardiovascular control.

The extrinsic control system consists of many control and feedback loops. The control loops are specifically responsible for adjusting arterial blood pressure via some of the cardiovascular variables that influence it. Figure 2-3 illustrates that arterial blood pressure is related to the overall blood flow from the heart or cardiac output CO and total peripheral vascular resistance R as follows:

$$P_a = CO \times R$$

where

$$\frac{1}{R} = \frac{1}{R_1} + \frac{1}{R_2} + \cdots + \frac{1}{R_N}.$$

Peripheral vascular resistance is adjusted by constriction or dilation of the resistance vessels respectively termed vasoconstriction ($\uparrow R$) or vasodilation ($\downarrow R$). The resistance vessels are primarily the arterioles whose thick, muscular walls allow for significant changes in caliber and thus resistance. Control of cardiac output is very complex and is dependent on many cardiovascular variables. However, it is normally adjusted by either modulation of heart rate or effective blood volume. In particular, cardiac output is a monotonically increasing function of heart rate and effective blood volume. Effective blood volume is defined to be the difference in total blood volume and the filling volume of the peripheral vasculature. Specifically, effective blood volume is adjusted by the constriction or dilation of the capacitance vessels respectively referred to as

venoconstriction (↑effective blood volume → ↑*CO*) or venodilation (↓effective blood volume → ↓*CO*). The capacitance vessels are the veins whose thin, muscular walls do not provide much resistance to flow but do allow for a greater capacity for changes in filling volume. The control mechanisms for adjusting peripheral vascular resistance, heart rate, and effective blood volume are of the following three types: local control, humoral control, and neural control. This thesis specifically focuses on the neural control which is on the time scale of seconds to minutes (short-term).

The autonomic nervous system is the portion of the nervous system that controls the involuntary functions of the body and consequently, plays a major role in the neural control of the cardiovascular variables that influence arterial blood pressure. The autonomic nervous system is divided into two subsystems, the sympathetic nervous system and the parasympathetic nervous system. The sympathetic nervous system innervates the arterioles and veins of the body along with the sinoatrial node (the heart's pacemaker), atria, and ventricles of the heart. The sympathetic nervous system can be further divided based on the particular chemical receptor in the tissue receiving the neural message. The chemical receptors are of three types, namely α, β_1, and β_2. The α receptors are present in the arterioles and veins and when stimulated, they cause vasoconstriction and venoconstriction. However, the β_2 receptors are also found in the arterioles and veins and when they are stimulated, they result in the opposing effect of vasodilation and venodilation. The β_1 receptors are present in the heart and when stimulated, they increase heart rate and enhance the contractility of the heart. The parasympathetic nervous system innervates the atria and ventricles of the heart to some extent but primarily innervates the sinoatrial and atrioventricular nodes via the vagus nerve. Parasympathetic stimulation decreases heart rate and slightly decreases the contractility of the heart.

There are a couple of points to note about these two subsystems. The first point to note is that the efferent branches of the sympathetic and parasympathetic nervous systems are tonically active. For example, modulation of sympathetic activity either increases or decreases vasoconstriction and venoconstriction with respect to a certain baseline tone.

Likewise, an increase or decrease in parasympathetic activity respectively decreases or increases heart rate. The second point to note is that the sympathetic nervous system increases its activity in the upright or tilted posture, while the parasympathetic nervous system increases its activity in the supine posture.

The feedback loops of the extrinsic control system work in conjunction with the control loops to maintain arterial blood pressure under various perturbations. The baroreceptor reflex is one of the most important feedback loops that act on the time scale of seconds to minutes (short-term). Baroreceptors are stretch receptors located in the carotid sinus and the aortic arch that sense changes in mean arterial blood pressure. An increase in pressure stretches the baroreceptors and causes them to transmit signals that eventually reach the autonomic nervous system. The autonomic nervous system responds by reducing peripheral vascular resistance via vasodilatory effects and decreasing cardiac output via venodilation and a reduction in heart rate and contractility of the heart. Of course, a decrease in arterial blood pressure sensed by the baroreceptors would result in the opposite effect. It should be noted that there are other inputs to the autonomic nervous system besides arterial blood pressure such as oxygen and carbon dioxide pressures and signals from higher brain centers.

2.3 Diabetic Autonomic Neuropathy

This section provides a brief treatment of the autonomic neuropathy associated with diabetes mellitus by summarizing material in [13,15,16,17]. Diabetes mellitus is a disease marked by excessive blood sugars due to insulin deficiency. Autonomic neuropathy, a frequent complication of diabetes mellitus, is a disorder that has damaging effects on sympathetic and parasympathetic nerves. Since this thesis deals with cardiovascular control mechanisms, this section specifically emphasizes the damage of the nerves that innervate the cardiovascular system referred to as cardiovascular neuropathy. Of course, cardiovascular neuropathy can have deleterious effects on the autonomic control mechanisms of the cardiovascular system.

The morphological changes associated with diabetic autonomic neuropathy and their pathogenesis are not well understood. Few studies of changes in morphology of the autonomic nerves have been completed because of the inaccessibility of these nerves. The issue of pathogenesis is controversial as both metabolic and vascular causations have been hypothesized. However, the clinical features of diabetic autonomic neuropathy are well recognized. These clinical features are often non-specific and range from mild disturbances to severe disabilities. They include symptoms involving the cardiovascular, gastrointestinal, and urogenital systems and disturbances to thermoregulatory function and pupillary reflexes.

In particular, the clinical features of cardiovascular neuropathy include postural hypotension and resting tachycardia. Postural hypotension is defined to be a fall in systolic blood pressure of greater than 30 mmHg when moving from the supine to standing posture. When the cardiovascular control system is operating normally, the decrease in arterial blood pressure that occurs on the move from supine to standing is sensed by the baroreceptors and ultimately peripheral resistance and cardiac output is increased mainly by the sympathetic nervous system. Therefore, postural hypotension reflects damage to predominantly sympathetic nerves. Resting tachycardia is a fast heart rate at rest and probably indicates the inability to reflexively modulate heart rate as a result of autonomic nerve damage.

Standard autonomic tests based on cardiovascular reflexes to various physiological perturbations are commonly employed to assess autonomic nerve damage. These tests assume that abnormal cardiovascular reflexes not only indicate cardiovascular neuropathy but damage throughout the entire autonomic nervous system. The goal of these tests are to confirm the presence and quantitatively assess the severity of autonomic neuropathy. These tests non-invasively assess the heart rate response to such perturbations as the Valsalva maneuver (subject blows into a mouthpiece at a pressure of 40 mm Hg for 15 seconds), standing up, and deep breathing and the blood pressure response to such perturbations as standing up and sustained handgrip. Although both branches of the autonomic nervous system are involved in these tests to some extent, the sympathetic nervous system is believed to play the major role in the blood pressure tests.

However, the blood pressure tests are relatively insensitive, particularly to early sympathetic nerve damage. Furthermore, both heart rate and blood pressure tests require the active cooperation of the subject and so, the test results may be difficult to reproduce.

The prevalence and natural history of diabetic autonomic neuropathy is not fully understood. Between 17 and 40% of randomly selected diabetic subjects have abnormal standard autonomic test results according to large studies. The development of clinical features is variable and appears to be relatively late. They are slowly progressive and usually irreversible and their onset often results in severe disabilities. Studies show that diabetic subjects with clinical symptoms of autonomic neuropathy are associated with considerable mortality. The potential consequences associated with diabetic autonomic neuropathy emphasize the need for its quantification. This quantification would provide a physiological measure of the progression of autonomic nerve damage and consequently, guidance for treatment. For example, an increase in the autonomic nerve damage would indicate the need for tighter glucose control. Therefore, the standard autonomic tests are often employed clinically despite their severe drawbacks. Clearly, a more sensitive test that requires minimal subject participation is needed to quantitatively assess diabetic autonomic neuropathy.

2.4 System Identification of Cardiovascular Control Mechanisms

This section discusses some aspects involved in the application of system identification to the study of short-term cardiovascular control mechanisms and presents some highlights of previous studies. Since a major component of this thesis is diabetic autonomic neuropathy, an emphasis is placed on the study of cardiovascular control mechanisms of subjects with diabetes mellitus.

2.4.1 Simple Models of Short-Term Cardiovascular Control Mechanisms

Figure 2-4 summarizes the autonomic control mechanisms of the cardiovascular system discussed in Section 2.2 in a block model The blocks of the model represent functional subsystems of the entire control system. The autonomic control mechanisms

are much too complicated for each block to be described with physical insight. However, if the input-output data to each subsystem could be measured, then system identification could be employed to estimate the dynamics of each block. Therefore, a fairly complete assessment of autonomic control would be obtained. Unfortunately, much of the input-output data in this model is not available for measurement and hence, this model is not particularly useful in the system identification context. However, some of the input-output data in this model, such as heart rate and arterial blood pressure, are easily accessible for measurement and can be used to estimate simpler models. Although, these models are not as detailed, they still provide useful insight about some aspects of autonomic control mechanisms.

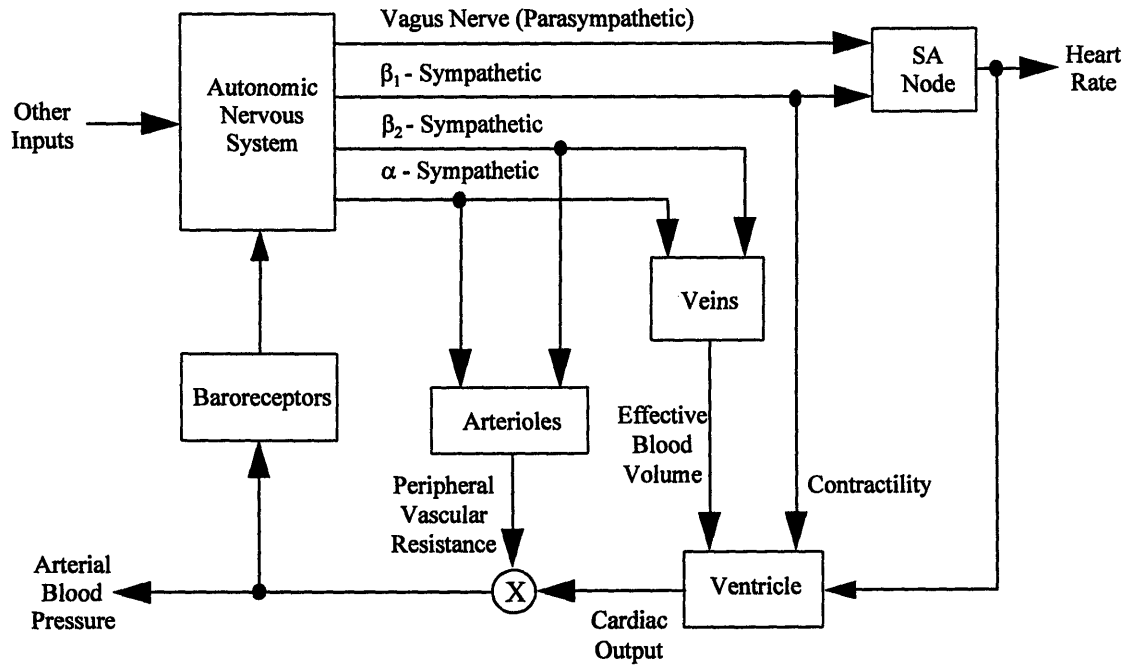

Figure 2-4: Block model of the autonomic control mechanisms of the cardiovascular system. Modified from [8].

Respiratory activity is also readily available for measurement via instantaneous lung volume. Although it is not included in the model in Figure 2-4, respiratory activity is an important factor in the study of cardiovascular control because it is a perturbation to

the cardiovascular system that causes a dynamic and compensatory response by the cardiovascular control mechanisms. Therefore, respiration can also be included in simple models of cardiovascular control. Specifically, respiration influences the cardiovascular system by perturbing both arterial blood pressure by mechanical mechanisms [8] and heart rate by autonomic mechanisms [37].

The intrathoracic pressure changes that result from respiration produce an additive effect on arterial blood pressure and modulate venous return and ventricular filling which eventually affect arterial blood pressure through their effects on cardiac output. Specifically, during inspiration, the intrathoracic pressure is more negative than usual. This causes an immediate decrease in arterial blood pressure due to capacitive effects and increases venous return to the right side of the heart which increases ventricular filling and eventually cardiac output from the left side of the heart. During expiration, the opposite effects occur.

Heart rate is also modulated by respiration. Specifically, phasic changes in heart rate follow the inspiratory and expiratory cycle of respiration. This is commonly referred to as respiratory sinus arrhythmia (RSA). The mechanisms that generate RSA are not completely understood; however, several potential mechanisms for RSA have been suggested. One possible mechanism is the direct neural coupling of the respiratory drive and heart rate control centers within the central nervous system. Another possible mechanism is the mechanical modulation of arterial blood pressure influencing heart rate via the baroreceptor reflex. Although the mechanisms for RSA are not completely understood, it is known that the modulation of heart rate in response to respiration is mediated by the autonomic nervous system almost exclusively.

2.4.2 Fluctuations in Cardiovascular Variables

It should be emphasized that when employing system identification to model the autonomic control mechanisms of the cardiovascular system, it is essential to deal with the fluctuations in cardiovascular variables such as heart rate, arterial blood pressure, and respiration about their mean values [3]. The mean values of cardiovascular variables are simple to examine and are thus used clinically, but they imply only the static state of

cardiovascular control. However, the fluctuations in cardiovascular variables about their mean values imply the dynamic nature of cardiovascular control as they represent the interplay between perturbations to the cardiovascular system and the response of cardiovascular control mechanisms. Of course, these perturbations can either be exogenous such as respiratory activity or endogenous such as local vascular resistance adjustments which affect total peripheral resistance.

The information concerning cardiovascular control inherent in the fluctuations in cardiovascular variables is illustrated by examining the power spectrum of heart rate. Power spectral estimation decomposes a signal into a sum of sine waves of different frequencies. The power spectrum is presented as the squared amplitude of these sine waves as a function of frequency. Figure 2-5 shows that a typical heart rate power spectrum contains three peaks that are centered at approximately 0.04 , 0.1, and 0.2 Hz. The 0.2 Hz peak is associated with fluctuations in respiration and the 0.1 and 0.04 Hz peaks are probably related to fluctuations resulting from arterial blood pressure regulation. The frequency band above 0.15 Hz is modulated by the parasympathetic nervous system as power in this band disappears during parasympathetic blockade. On the other hand, the frequency band below 0.15 Hz is modulated by both sympathetic and parasympathetic nervous systems as power in this band is diminished during either blockade and completely disappears during double blockade.

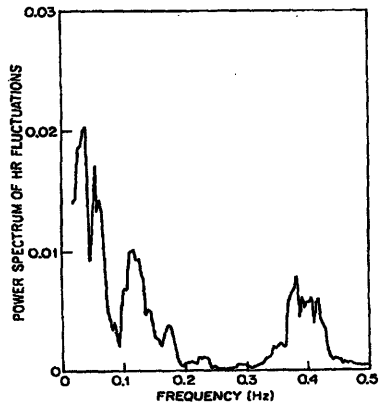

Figure 2-5: Sample power spectrum of heart rate fluctuations. Reproduced from [1].

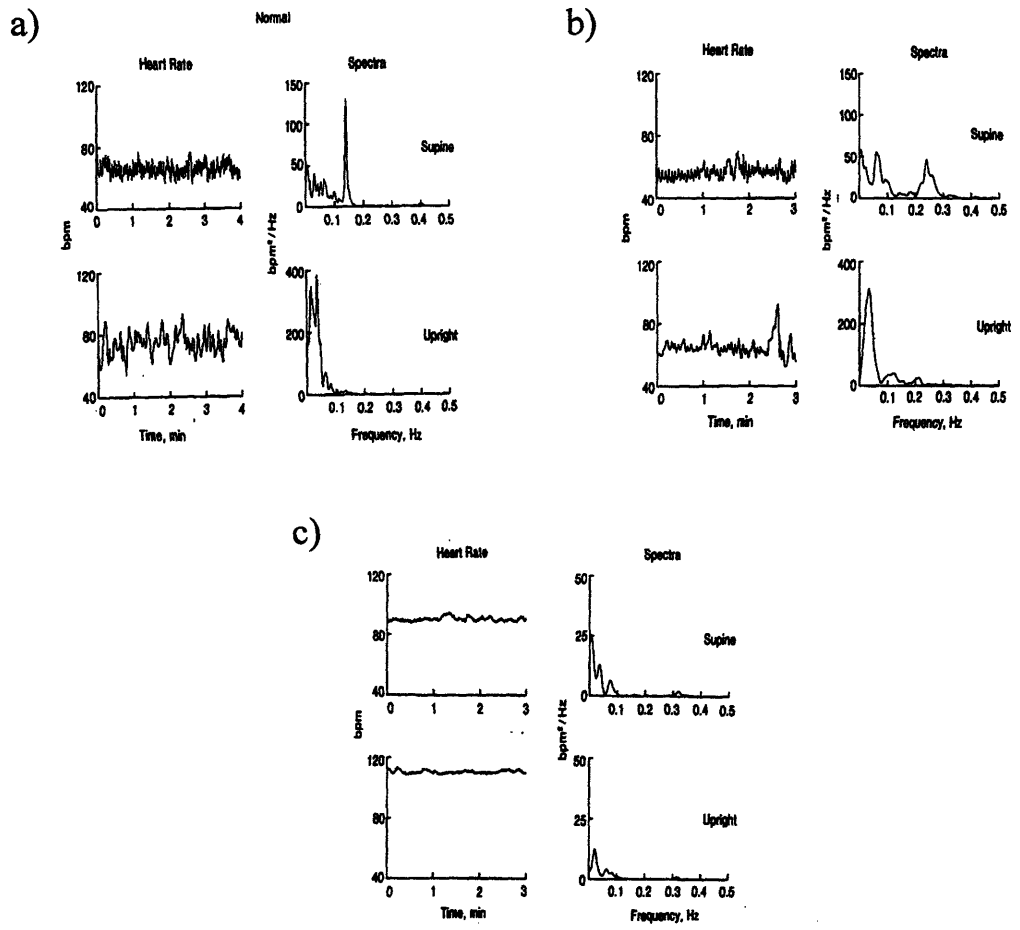

Figure 2-6: The power spectrum of heart rate for a) a control, b) a diabetic subject with moderate autonomic neuropathy, and c) a diabetic subject with severe autonomic neuropathy. Reproduced from [20].

Since the power spectrum reveals so much about autonomic control, it is natural to wonder whether it can be used as an assessment tool for autonomic neuropathy. In fact, there has been extensive work on the application of heart rate power spectral estimation to assess the autonomic neuropathy associated with diabetes mellitus [7,20,27,33]. The total power of the heart rate spectrum decreases with increasing autonomic neuropathy. This is consistent with the hypothesis that autonomic modulation of heart rate reduces as nerve damage progresses. Figures 2-6a, b, and c illustrate this

trend by respectively showing the power spectrum of a control subject, a subject with moderate autonomic neuropathy, and a subject with severe autonomic neuropathy in both supine and upright postures. Additionally, the parameters of the heart rate power spectrum such as low frequency power, high frequency power, and total power compare well with the standard autonomic tests. Although heart rate power spectral analysis is a quantitative, non-invasive, and sensitive method that requires minimal subject participation, it only provides information about an output of a control loop of the cardiovascular control system. It does not provide any information about how the output would change to varying inputs to the control loop. Clearly, it would be more informative to estimate the dynamics of the couplings of the control and feedback loops of the cardiovascular control system from experimental data.

2.4.3 Previous Studies

Many previous studies have applied system identification to quantitatively and non-invasively assess cardiovascular control mechanisms with minimal subject participation. A few of these studies have specifically assessed the cardiovascular control mechanisms of diabetic autonomic neuropathy. Of course, none of these studies provide a complete description of cardiovascular control; however, they do provide insight about some aspects of the cardiovascular control system. It should be noted that all of these studies assumed that the cardiovascular control mechanisms behaved as LTI systems. The system identification techniques that have been employed can be divided essentially into two categories namely, nonparametric transfer function analysis and parametric system identification.

Nonparametric transfer function analysis provides an estimation of the gain and phase delay as a function of frequency between a single input and output of an LTI system. Because this type of analysis applies to LTI systems, a requirement is that the input data contains all relevant frequencies of interest so that the system can be identified at all these frequencies. The estimation procedure involves the determination of the optimal estimate of the transfer function in the least squares sense computed via FFT-

based spectral analysis. The interested reader can find a detailed treatment of this topic in [38].

Nonparametric transfer function analysis has been applied to analyze several aspects of cardiovascular control. Berger et al. stimulated the vagus and cardiac sympathetic nerves of dogs in a broadband manner to study the coupling of this stimulation and the resulting atrial rate in order to gain insight about the dynamics of the sinoatrial node [10]. They found that the sinoatrial node behaves as a lowpass filter whose cutoff frequency depends on both the mean level of stimulation and the particular nerve that was stimulated. Saul et al. examined the coupling of respiration and heart rate using techniques to broaden the frequency content of respiration in order to study RSA [35]. They determined that RSA was frequency dependent with parasympathetic nervous control providing a faster and larger heart rate response to respiration than sympathetic nervous control. The objective of study in [36] included the analysis of RSA and the coupling between respiration and blood pressure by blocking branches of the autonomic nervous system pharmacologically. One of the discoveries of this study was that the respiratory effects on arterial blood pressure are mediated by both RSA and the mechanical affects of respiration on arterial blood pressure. Freeman et al. assessed RSA in diabetic autonomic neuropathy [21]. The main results of this study are shown in Figure 2-7. Figure 2-7a shows the mean gain between respiration and heart rate as a function of frequency for groups with varying degrees of autonomic neuropathy. Specifically, the mean gain decreases as autonomic neuropathy increases across these groups for both the supine and tilted postures. Figure 2-7b illustrates the mean phase delay between respiration and heart rate as a function of frequency for these groups. The phase delay at low frequencies is particularly of interest and implies that sympathetic modulation increases (but to no avail as is evident in Figure 2-7a) with increasing autonomic neuropathy in the supine posture and plays a major role regardless of the degree of autonomic neuropathy in the tilted posture.

Clearly, nonparametric transfer function analysis provides useful insight about cardiovascular control mechanisms. However, its utility is limited. Consider the important coupling between heart rate and arterial blood pressure. This coupling is a

closed-loop relationship in that arterial blood pressure influences heart rate by way of the autonomically mediated baroreceptor reflex, and heart rate affects arterial blood pressure via the mechanical effects of ventricular contraction. As will be shown in Section 3.4.2, causality conditions must be imposed in order to identify the open-loop couplings in a closed-loop system. Since nonparametric transfer function analysis cannot impose causality conditions, this technique cannot distinguish between the open-loop couplings in a closed-loop system. However, as will be shown in Section 3.2.1, parametric system identification can impose causality conditions. The power of parametric system identification over nonparametric transfer function analysis rests with this fact.

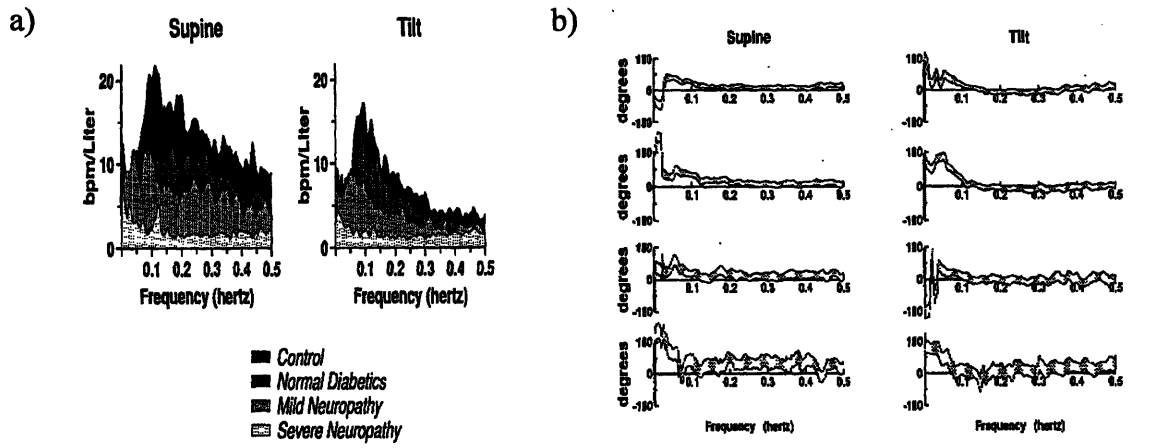

Figure 2-7: a) The mean transfer function gain between respiration and heart rate for groups with varying degrees of neuropathy in the supine and tilted postures. b) The mean transfer function phase delay between respiration and heart rate for these groups also in the supine and tilted postures with the control, normal diabetic, mild neuropathy, and severe neuropathy groups respectively arranged from top to bottom. Reproduced from [21].

Parametric system identification provides an estimation of couplings typically in the form of a parameterized impulse responses. The general estimation procedure is reviewed in Section 2.1.3. Of course, parametric system identification can also be applied to open-loop couplings. Yana et al. examined RSA by blocking branches of the autonomic nervous system pharmacologically [45]. Their technique included a method to

broaden the frequency content of respiration so as to provide informative data, pre- and post-processing procedures, a time domain, moving average (MA) difference equation, and least squares estimation. Their model estimates in the form of impulse responses implied that changes in heart rate anticipated changes in respiration. This suggests the neural coupling of respiratory drive and heart rate control centers and thus supports the role of the central nervous system in the generation of RSA. They also found that parasympathetic block almost completely diminished the impulse response while sympathetic block had little effect, perhaps indicating greater parasympathetic modulation.

As mentioned previously, the real utility of parametric system identification in the cardiovascular control context is that it can be applied to closed-loop systems. Kenet examined the closed-loop coupling of heart rate and arterial blood pressure in dogs under normal sinus rhythm and during atrial fibrillation [26]. This technique involved using a symmetric closed-loop model, autoregressive, moving average (ARMA) difference equations, and generalized least squares estimation. He found that the data was not informative enough during normal sinus rhythm; however, during atrial fibrillation this problem was resolved at the expense of normal operating conditions. Baselli et al. studied the couplings between heart rate, arterial blood pressure, and respiration [6]. Their method involved using a closed-loop model consisting of seven transfer relations and two unmeasured noise perturbations, dividing the system into two models, and generalized least-squares estimation. However, the data was not informative enough as the respiration data was not persistently exciting. Appel et al. also examined the couplings between heart rate, arterial blood pressure, and respiration under selective pharmacological blockade of autonomic pathways [4]. This method involved a random-interval breathing technique to provide informative data, a closed-loop model consisting of four transfer relations and two unmeasured noise perturbations, ARMA difference equations, and least squares estimation. Their method was able to distinguish between altered autonomic states produced by both postural changes and the pharmacological blockade. Additionally, their results were consistent with established physiological

experimental results. This thesis, in fact, implements this same method to study aspects of the cardiovascular control mechanisms of patients with diabetic autonomic neuropathy.

Chapter 3

Closed-Loop System Identification Procedure

This chapter describes the closed-loop system identification procedure that is implemented to assess diabetic autonomic neuropathy. The chapter presents this procedure in the context of the general system identification procedure in Section 2.1.3. Specifically, input-output data generation, candidate model selection, "best" model determination, and model validation are all discussed in some detail.

3.1 Generation of Input-Output Data

The first step in any system identification procedure is to create the input-output data. This step includes experiment design and data collection and processing. The objective is to generate the most informative, cleanest data possible so that good models can be constructed.

3.1.1 Experiment Design

Experiment design deals with such issues as what signals to measure, under what conditions are these signals to be measured, and whether these signals are related in open-

or closed-loop. Since heart rate, arterial blood pressure (ABP), and instantaneous lung volume (ILV) signals are all easily accessible and identification of their couplings can provide useful insight about cardiovascular control mechanisms, these signals are chosen for measurement. Strictly speaking, heart rate is not readily available, but it can be derived from the surface electrocardiogram (ECG) which is perhaps the easiest cardiovascular signal to measure. Therefore, the ECG, ABP, and ILV signals are actually chosen for measurement. These signals are measured during two sessions, first while the subject is supine and then following passive tilting to 60° (relative to the supine posture) by an electrically driven tilt table. Each posture provides a different balance between sympathetic and parasympathetic control of the cardiovascular system. Consequently, the measurements from each session may be very insightful about the roles of the sympathetic and parasympathetic nervous systems in cardiovascular control. Before each of these sessions, the subject is provided with a period of hemodynamic equilibration. Approximately eight minutes of data are measured for each session as it is short-term cardiovascular control mechanisms that will be assessed. It should be emphasized that this is a closed-loop experiment because of the relationship between heart rate and ABP.

The goal of experiment design is to obtain maximally informative data. Informative data results from persistently exciting inputs, and in practice, persistently exciting inputs correspond to broadband inputs. (This issue will be discussed further in Section 3.4.2.) Heart rate and ABP can be thought of as outputs of the cardiovascular control system; however, ILV is an exogenous input to this system. Therefore, it is essential for ILV to be broadband. Unfortunately, normal breathing patterns typically result in narrowband ILV data. As a result, during both sessions, subjects are instructed to breathe on cue according to a sequence of auditory tones spaced by independent and identically distributed, modified exponential inter-breath times. The inter-breath times range from one to 15 seconds with a mean of five seconds to avoid subject discomfort. This "random-interval breathing technique" provides broadband ILV data within 0.5 Hz while preserving normal ventilation [9]. Figure 3-1 illustrates the effectiveness of the

random-interval breathing technique by showing the power spectra of ILV generated by normal breathing and random-interval breathing.

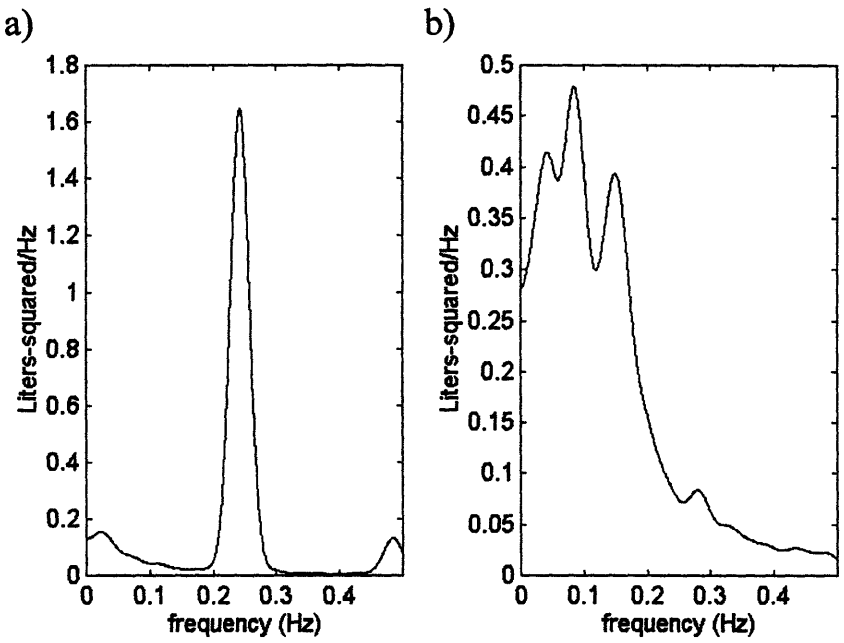

Figure 3-1: ILV power spectra from a) normal breathing and b) random-interval breathing.

3.1.2 Data Collection and Processing

The collection and processing of data involves the measurements and signal processing techniques included in the generation of the input-output data. The ECG, ABP, and ILV signals are measured non-invasively and recorded continuously on a Teac C-71, eight-channel FM tape recorder (Teac America, Montebello, CA). The ECG signal is measured with a Hewlett-Packard EKG Monitor 78203A (Andover, MA); the ABP signal is measured with a 2300 Finapress Continuous Blood Pressure Monitor (Ohmeda, Fort Lee, NJ); and the ILV signal is measured with a two-belt chest-abdomen inductance pelthysmograph (Respitrace System, Ambulatory Monitoring, Inc., Ardsley, NY). The ILV signal is calibrated by having the subject alternately empty and fill an 800 ml bag after each period of hemodynamic equilibration. These three signals are then lowpass

filtered at 180 Hz with a six-pole Butterworth filter and digitized with a 12 bit bipolar A/D converter at a sampling rate of 360 Hz. Figure 3-2 shows a sample trace of the resulting digitized ECG, ABP, and ILV signals.

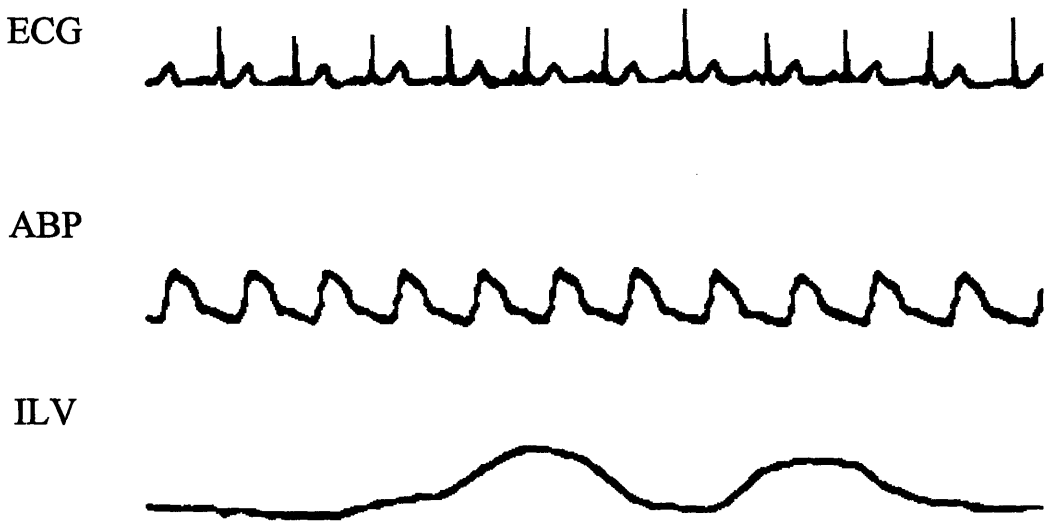

Figure 3-2: Sample 7.5 second trace of digitized ECG, ABP, and ILV data.

The couplings of the three digitized signals can be described with the closed-loop model of short-term cardiovascular control illustrated in Figure 3-3. The model represents the closed-loop coupling of heart rate and ABP with ILV as an exogenous perturbation that directly influences both heart rate and ABP. Since, it is assumed that heart rate and ABP do not affect ILV, these couplings are not included in the model. Therefore, the model contains four unknown open-loop couplings or transfer relations (ILV→HR, BAROREFLEX, ILV→ABP, and CIRCULATORY MECHANICS) and two unmeasured noise perturbations (N_{HR} and N_{ABP}). ILV→HR represents the autonomic coupling between ILV and heart rate or equivalently, RSA. BAROREFLEX represents the effects of ABP on heart rate due to the autonomically mediated baroreceptor reflex. ILV→ABP represents the mechanical coupling between ILV and ABP resulting from variations in intrathoracic pressure induced by respiration producing an additive effect on

ABP and modulating venous return and ventricular filling which indirectly affect ABP. CIRCULATORY MECHANICS primarily represents the mechanical effects of a single ventricular contraction on the ABP waveform. However, the autonomic nervous system also has some influence on CIRCULATORY MECHANICS since the ABP waveform is dependent on peripheral vascular resistance which is sympathetically mediated. N_{HR} and N_{ABP} respectively represent the residual variation in HR and ABP not accounted for by the couplings.

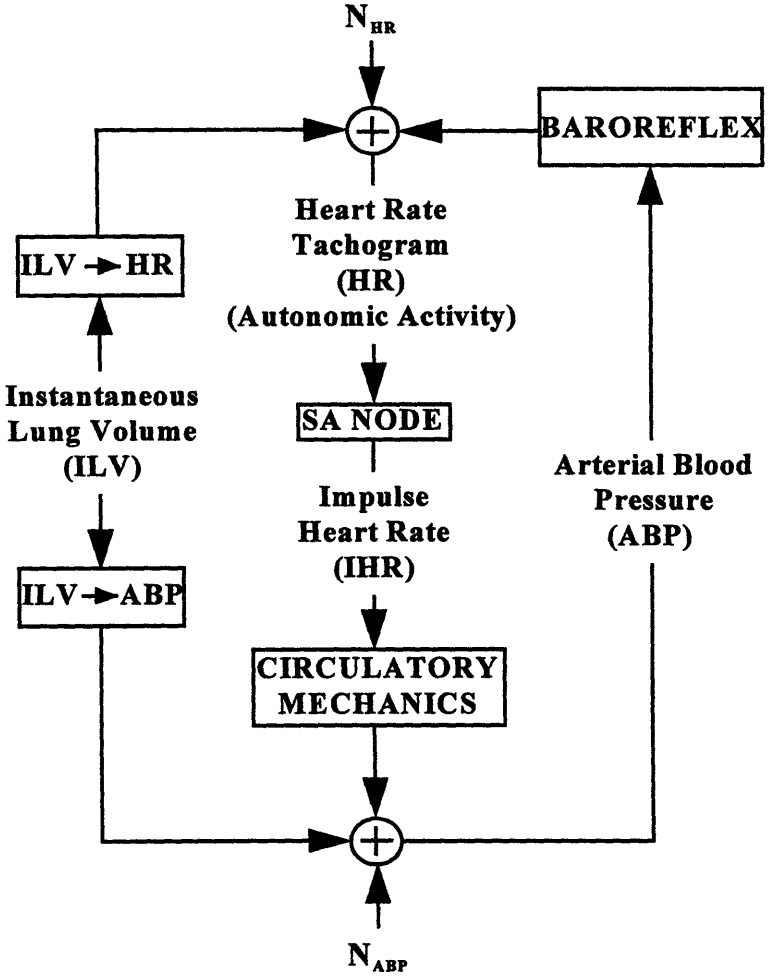

Figure 3-3: Closed-loop model of short-term cardiovascular control mechanisms relating heart rate, ABP, and ILV.

An additional transfer relation (SA NODE) is also included in the model. SA NODE reflects the effects of autonomic tone (represented by a heart rate tachogram (HR)) on the modulation of the timing of ventricular contractions (represented by an impulse heart rate (IHR) signal) by the sinoatrial node. Since the dynamics of the sinoatrial node are well described via the integral pulse frequency modulation (IPFM) model [25] and HR and IHR can be derived from the ECG as described in [11] and illustrated in Figure 3-4, SA NODE is not estimated. The SA NODE is essential to the model, though. The autonomic modulation of HR is over the spectral band between dc and roughly 0.35 Hz [31], while the spectral content of the ABP waveform includes up to the tenth harmonic of the mean heart rate which is usually about 10 Hz [12]. However, it will be assumed that the couplings are LTI and so, the output can only contain power at frequencies that are excited by the input. Because the spectral content of IHR also includes at least up to the tenth harmonic of the mean heart rate, the function of SA NODE is to close the loop by converting HR to IHR which is in turn linearly coupled to the ABP waveform. Thus, SA NODE is a fully defined nonlinear element which is crucial to the closed-loop model but does not require estimation.

It will be discussed in Section 3.3.1 that the couplings and noise perturbation involved in the generation of HR will be estimated separately from the couplings and noise perturbation involved in the creation of ABP. The signals used for the estimation of the former couplings and noise perturbation are HR, ABP, and ILV. This data is zero-meaned and decimated to 1.5 Hz which is more than sufficient to accommodate the spectral content of the autonomic modulation of HR. The longest portion of the eight minute data segment that is clean is used for this estimation. The signals used for the estimation of the latter couplings and noise perturbation are ABP, IHR, and ILV. This data is zero-meaned and decimated to 90 Hz which provides more than enough bandwidth for the ABP waveform. Ninety seconds of the cleanest portion of the eight minute data segment is used for this estimation. Additional processing techniques will be necessary in the closed-loop system identification procedure; however, these techniques will be discussed in Section 3.4.3.

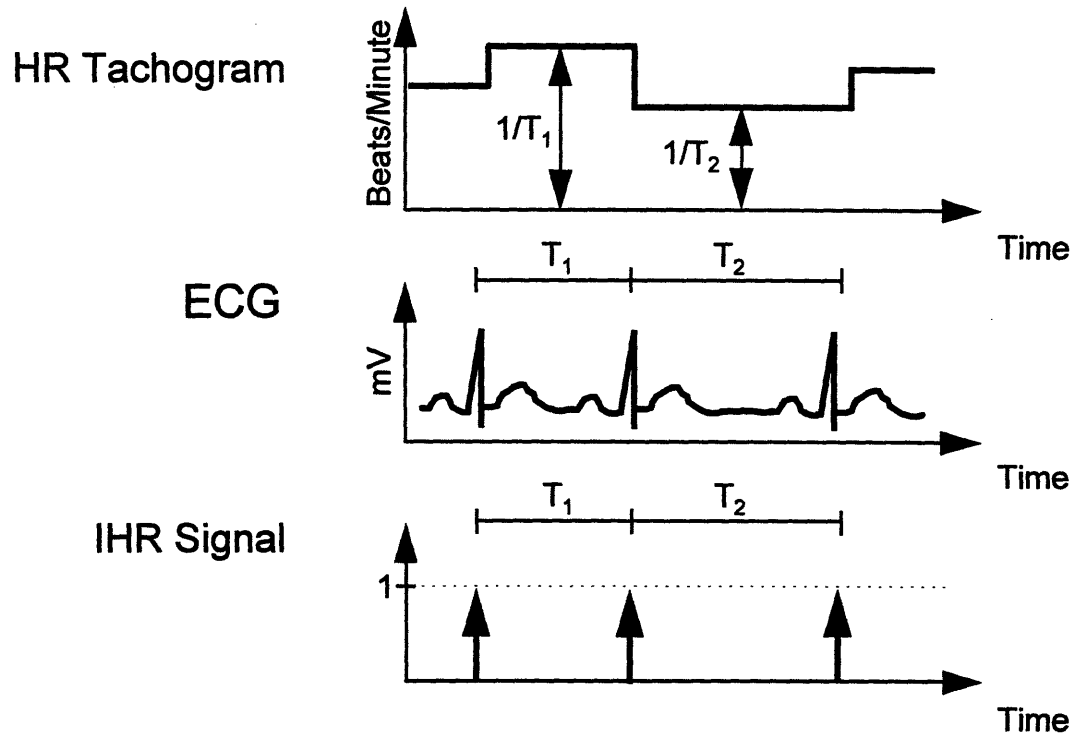

Figure 3-4: Derivation of the heart rate tachogram (HR) and the impulse heart rate signal (IHR) from the ECG. The units of ECG are in millivolts (mV), while IHR has arbitrary units.

3.2 Least Squares Estimation

The next step of the general system identification procedure deals with the selection of a candidate set of models. However, the fundamental concepts of least squares estimation are presented here, because they are essential to understanding this step and the remaining steps of the closed-loop system identification procedure. Least squares estimation is an identification method that is used in this thesis as a tool for the determination of the "best" model. Since the closed-loop system identification procedure employs LTI systems in the form of difference equations, this section specifically focuses on least squares estimation in this context.

3.2.1 LTI Systems

Disregarding any disturbances, a system is a transformation $T\{\cdot\}$ that maps an input $u(t)$ to an output $y(t)$ i.e.,

$$y(t) = T\{u(t)\}.$$

A linear system follows the principle of superposition which states that

$$T\{au_1(t) + bu_2(t)\} = aT\{u_1(t)\} + bT\{u_2(t)\}$$

where $u_1(t)$ and $u_2(t)$ are inputs to the linear system and a and b are arbitrary constants. A time-invariant system is one in which a time shift of the input produces the identical time shift of the output. Equivalently, provided that the output $y(t)$ of a system results from the input $u(t)$, a system is time-invariant if the input $u(t-t_0)$ produces the output $y(t-t_0)$. The input-output relationship of an LTI system is described by the convolution operation as follows:

$$y(t) = \sum_k h(k)u(t-k) = h(t)*u(t)$$

where $*$ denotes the convolution operator and $h(t)$ is referred to as the impulse response of the LTI system. Note that if the impulse response of an LTI system is known, then for any input to that system, the output can be determined. In other words, the impulse response completely characterizes an LTI system. This is a powerful feature of LTI analysis.

An important subclass of LTI systems are linear constant coefficient difference equations (LCCDE's). The general form of such a difference equation with input $u(t)$ and output $y(t)$ is

$$\sum_{k=R'}^{R} a_k y(t-k) = \sum_{k=S'}^{S} b_k u(t-k).$$

where $R' \leq 0$. Note that if $R' = 0$ and $S' \geq 0$, the system is causal. This general form is often referred to as an autoregressive, moving average (ARMA) equation. Assuming $R' = 0$, the autoregressive (AR) portion of this equation deals with past values of the output influencing the present value of the output. The moving average (MA) portion of

the equation deals with the present value of the output being affected by some weighted average of the input sequence. The a_k's are called the AR parameters, while the b_k's are referred to as the MA parameters. If S', $S = 0$, then the difference equation is purely AR. However, if R', $R = 0$, then the difference equation is purely MA. In this case, the difference equation is equivalent to the convolution operation with the b_k's being the impulse response. It should be noted that the values of R', R, S', and S are referred to as the order of the difference equation in this thesis and that these values directly relate to the parameterization. Of course, LCCDE's can be extended to the multi-input case as will be shown in the next section. A more detailed treatment of LTI systems and LCCDE's can be found in [32].

3.2.2 Formulation of the Least Squares Problem

The least squares problem in the closed-loop system identification context has two components, input-output data and a difference equation. Section 3.1 discussed the generation of input-output data, and the selection of candidate models in the form of difference equations will be presented in Section 3.3. More precisely, these two components lead to the formulation of the least squares problem. Consider the following two input ARMA equation which can serve as a model of a dynamic system:

$$y(t) = \sum_{k=1}^{R} a_k y(t-k) + \sum_{k=0}^{S} b_{1k} u(t-k) + \sum_{k=0}^{T} b_{2k} x(t-k) + e(t)$$

where $e(t)$ represents unobserved noise and is referred to as the residual error. The residual error accounts for both imperfections in the measurement process and dynamics of the true system not contained in the model. Additionally, assume that there are $N+\max(R,S,T)$ samples of the input-output data: $u(t)$, $x(t)$, and $y(t)$ where $t \in [-\max(R,S,T)+1, N]$.

This ARMA equation can also be written in the following vector product form:

$$y(t) = \phi^{\mathrm{T}}(t)\theta + e(t) \tag{3.1}$$

where

$$\phi^{\mathrm{T}}(t) = [y(t-1)\cdots y(t-R) \quad u(t)\cdots u(t-S) \quad x(t)\cdots x(t-T)]$$

$$\theta^T = [a_1 \cdots a_R \quad b_{11} \cdots b_{1S} \quad b_{21} \cdots b_{2T}].$$

$\phi^T(t)$ and θ are respectively referred to as the data vector and the parameter vector. Since $t \in [-\max(R,S,T)+1, N]$, there are N such equations that can be placed in the following matrix form:

$$Y = \Phi\theta + E$$

where

$$Y^T = [y(1)\ y(2) \cdots y(N)]$$

$$\Phi^T = [\phi(1)\ \phi(2) \cdots \phi(N)]$$

$$E^T = [e(1)\ e(2) \cdots e(N)].$$

Disregarding E for the moment, a system of N equations and $M = R+S+T+2$ unknown parameters results. Typically $N > M$, or equivalently, the number of the samples of data is larger than the number of parameters of the difference equation. Therefore, the system of equations is overdetermined and an exact solution for the parameters generally does not exist. One can then resort to the least squares solution, and so the formulation of the least squares problem is complete.

3.2.3 Derivation of the Least Squares Estimate

Least squares determines the parameters of the difference equation by fitting the input-output data to the equation in the least squares sense. This amounts to minimizing the mean-squared difference between the actual output $y(t)$ and the output produced by the model estimate $\phi^T(t)\theta$. The output produced by the model estimate will henceforth be referred to as the prediction. By rearranging (3.1), this difference is found to be the residual error

$$e(t) = y(t) - \phi^T(t)\theta.$$

The mean-squared residual error is called the loss function V and is defined as follows:

$$V = \frac{1}{N}\sum_{t=1}^{N} e^2(t) = \frac{1}{N}E^T E = \frac{1}{N}\|E\|^2 = \frac{1}{N}\|Y - \Phi\theta\|^2.$$

The minimization of V can be achieved via the Orthogonal Projection Theorem. This theorem states that the prediction vector $\Phi\theta$ minimizes V provided that the residual error vector E is orthogonal to all possible prediction vectors or equivalently, the column space of Φ. The proof of this theorem is very simple. Let Y' be the prediction vector for which $E=Y-Y'$ is perpendicular to the column space of Φ. If Y'' is any prediction vector, then

$$V = \frac{1}{N}\|Y-Y''\|^2 = \frac{1}{N}\|(Y-Y')+(Y'-Y'')\|^2 = \frac{1}{N}\|Y-Y'\|^2 + \frac{1}{N}\|Y'-Y''\|^2$$

where the last equality is from the Pythagorean Theorem and the fact that $Y-Y'$ is orthogonal to $Y'-Y''$ which is clearly in the column space of Φ. Obviously, $Y''=Y'$ minimizes V. Figure 3-5 provides a two dimensional geometric perspective of this result.

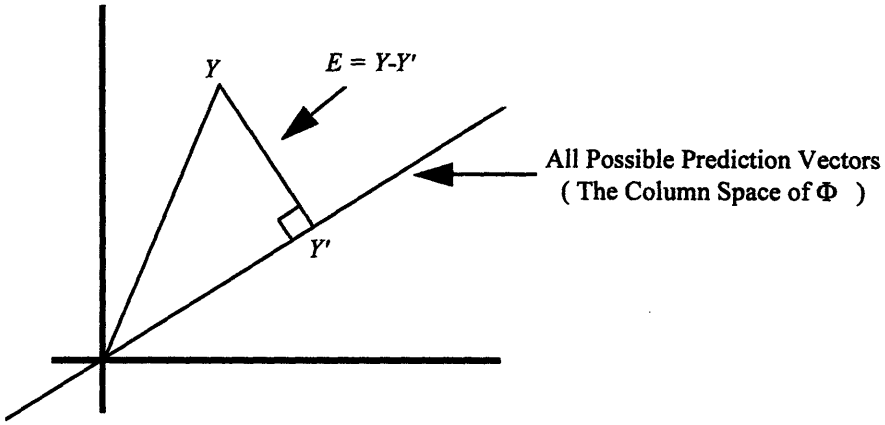

Figure 3-5: Two dimensional geometrical perspective of the Orthogonal Projection Theorem. Modified from [44].

The least squares estimate $\hat{\theta}$ can now easily be derived. Since E must be orthogonal to $\Phi\hat{\theta}$, it follows that

$$E^T\Phi\hat{\theta} = (Y-\Phi\hat{\theta})^T\Phi\hat{\theta} = 0.$$

The solution of this equation results in the least squares estimate

$$\hat{\theta} = (\Phi^T\Phi)^{-1}\Phi^T Y. \qquad (3.2)$$

3.2.4 Consistency Conditions for the Least Squares Estimate

A crucial requirement for the least squares estimate is that it is consistent. Assume that the dynamics of the true system can be described as follows:

$$Y = \Phi\theta_0 + E \tag{3.3}$$

where the vector θ_0 contains the true parameters. Then the least squares estimate (or any estimate for that matter) is consistent if

$$\hat{\theta} \to \theta_0 \ as \ N \to \infty.$$

As mentioned in Section 2.1.3, if the estimate is consistent then the system is said to be identifiable. The issue of consistency can be analyzed by substituting for Y in (3.2) with (3.3) as follows:

$$\hat{\theta} = (\Phi^T\Phi)^{-1}\Phi^T(\Phi\theta_0 + E).$$

After further simplification,

$$\hat{\theta} = \theta_0 + (\Phi^T\Phi)^{-1}\Phi^T E.$$

This equation can be written in terms of vectors as follows:

$$\hat{\theta} = \theta_0 + \left[\frac{1}{N}\sum_{t=1}^{N}\phi(t)\phi^T(t)\right]^{-1}\left[\frac{1}{N}\sum_{t=1}^{N}\phi(t)e(t)\right]. \tag{3.4}$$

The data $u(t)$, $x(t)$, and $y(t)$ are assumed to be jointly, wide-sense stationary (WSS) stochastic processes that are ergodic with respect to second order moments. WSS stochastic processes have second-order statistics that are time-invariant i.e., the mean of the process does not vary with time and the covariance of the process only depends on a time difference. Jointly, WSS processes additionally have cross-covariances that are time-invariant. Jointly, WSS processes that are ergodic with respect to second order moments have the following property:

$$\frac{1}{N}\sum_{t=1}^{N} w(t)z(t+\tau) \to E(w(t)z(t+\tau)) \text{ as } N \to \infty$$

where $E(\cdot)$ is the expectation operator and $w(t)$ and $z(t)$ are any jointly, WSS processes. In other words, the WSS process varies enough over time so that second order ensemble behavior can be inferred from time averages. These assumptions hold under fairly weak

conditions and are assumed in this thesis. A detailed discussion of this issue can be found in [39]. Therefore, the sums in (3.4) tend to expected values as $N \to \infty$ as follows:

$$\hat{\theta} = \theta_0 + \left\{E(\phi(t)\phi^T(t))\right\}^{-1} E(\phi(t)e(t)).$$

Therefore, $\hat{\theta}$ is consistent if both of the following two conditions hold:

1) $E(\phi(t)\phi^T(t))$ is nonsingular, and

2) $E(\phi(t)e(t)) = 0$.

Of course, $E(\phi(t)\phi^T(t))$ is defined to be the covariance matrix of $\phi(t)$. An excellent, thorough treatment of least squares estimation can be found in [39].

3.3 Selection of a Candidate Set of Models

The issues involved in the selection of a candidate set of models can now be presented. This step is typically the most difficult of the general system identification procedure, particularly when a black box approach is taken. As discussed in Section 2.1.3, a black box approach deals with selecting a candidate set of models without regard to physical laws. In this approach, the parameters of the models are viewed simply as a means to fit the data. Since the cardiovascular control mechanisms are too complex to be modeled with physical insight, the black box approach must be taken here.

3.3.1 MA Difference Equations

As mentioned in Section 1.1, studies have shown that the cardiovascular control system displays both nonlinear and time-varying behavior. However, LTI analysis is often employed to study aspects of this system. There are essentially two reasons for this. The first reason is that LTI analysis is a well developed, powerful tool for the study of systems. The second reason deals with the character of the cardiovascular signals that are often examined for the study of the cardiovascular control system. It is hypothesized that the under stable experimental conditions, the fluctuations in these signals about their mean values are small enough so that the couplings between these fluctuations can be related in an LTI fashion. A more detailed discussion of this hypothesis can be found in [2].

As discussed in Section 3.1, the input-output data used in the closed-loop system identification procedure is generated under stable experimental conditions. Therefore, the "true" description of the open-loop couplings in the closed-loop model of short-term cardiovascular control in Figure 3-3 is hypothesized to be LTI. This closed-loop model can conveniently be divided into two parts, namely the generation of HR and the creation of ABP. Consequently, N_{HR} and the two transfer relations associated with HR generation can be treated separately from N_{ABP} and the two transfer relations associated with the creation of ABP. Thus, two difference equations can describe the closed-loop model. Since all the transfer relations in the closed-loop model are considered LTI, it is assumed that the generation of HR and ABP each involve the sum of two convolutions and a noise perturbation. In accord with the closed-loop model, the difference equations that describe the "true" dynamics of the system are as follows:

$$HR(t) = \sum_{k=1}^{R} b_{1k} ABP(t-k) + \sum_{k=S'}^{S} b_{2k} ILV(t-k) + N_{HR}(t) \tag{3.5}$$

$$ABP(t) = \sum_{k=1}^{T} c_{1k} IHR(t-k) + \sum_{k=U'}^{U} c_{2k} ILV(t-k) + N_{ABP}(t) \tag{3.6}$$

with $R, S, T, U = \infty$ as it seems unlikely that the "true" dynamics of such a complicated system could be represented with a finite number of parameters. The residual errors $N_{HR}(t)$ and $N_{ABP}(t)$ are assumed to be colored processes that are uncorrelated with each other and with $ILV(t)$. These two equations are referred to as two-input MA equations. Note that only the past values of the $\{ABP(t)\}$ sequence influence $HR(t)$, and only the past values of the $\{IHR(t)\}$ sequence affect $ABP(t)$. Since the sinoatrial node is a causal system, $IHR(t)$ is dependent on only present and past values of the $\{HR(t)\}$ sequence. Therefore, (3.5) and (3.6) restrict the closed-loop part of the model in Figure 3-3 to be strictly causal. It should be noted that most physical closed-loop systems are strictly causal and so, this assumption is quite reasonable. The importance of strictly causal closed-loop equations in the context of least squares estimation will be discussed in Section 3.4.2.

Since (3.5) and (3.6) are assumed to describe the "true" dynamics of the closed-loop model, it would seem appropriate to choose the form of these difference equations

and a set of finite parameterizations for the candidate set of models. However, it turns out that applying least squares to either of these equations (as they are estimated separately) results in inconsistent parameter estimates. In fact, any closed-loop system whose open-loop couplings are described by MA equations and colored residual errors cannot be estimated consistently with least squares and MA equations. For example, consider the simpler closed-loop system in Figure 3-6 whose true dynamics are represented by the following two MA equations:

$$y(t) = \sum_{k=1}^{P} h_{1k} x(t-k) + N_y(t) \tag{3.7}$$

$$x(t) = \sum_{k=1}^{Q} h_{2k} y(t-k) + N_x(t) \tag{3.8}$$

where P, $Q = \infty$ and the residual errors $N_y(t)$ and $N_x(t)$ are colored processes that are uncorrelated with each other. Now consider the form of these equations and a set of finite parameterizations as a possible candidate set of models. In order to check for the consistency of the least squares estimation of the form of such equations, (3.7) is written in vector product form as follows:

$$y(t) = \phi^{\mathrm{T}}(t)\theta + N_y(t)$$

where

$$\phi^{\mathrm{T}}(t) = [x(t-1)\ x(t-2)\cdots x(t-P)]$$

$$\theta^{\mathrm{T}} = [h_{11}\ h_{12}\cdots h_{1P}].$$

From Section 3.2.4, one condition for consistency in this case is that the vector $E(\phi(t)N_y(t)) = 0$. The elements of the $\phi(t)$ vector all contain contributions from past values of the $\{y(t)\}$ sequence (see (3.7)) and thus the past values of the $\{N_y(t)\}$ sequence (see (3.8)). Since $N_y(t)$ is a colored process (i.e., it is correlated in time), the elements of $E(\phi(t)N_y(t))$ cannot be zero and so, consistent parameter estimates cannot be obtained with this form of difference equation as a direct consequence of the closed-loop. By a similar argument, least squares estimation of the parameters of (3.8) also cannot be consistent.

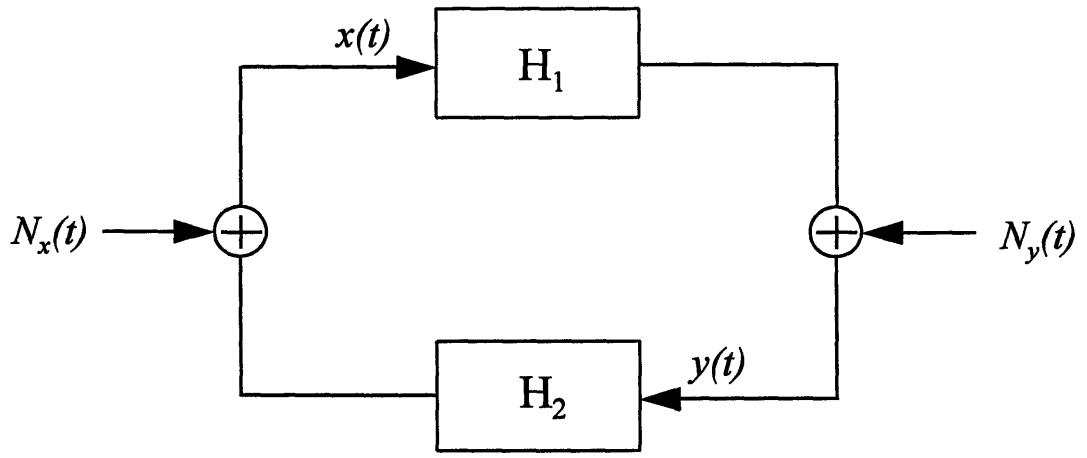

Figure 3-6: Simple closed-loop system in which the dynamics of the couplings between $x(t)$ and $y(t)$ represented by H_1 and H_2 are described by MA equations and the residual errors $N_y(t)$ and $N_x(t)$ are colored.

3.3.2 ARMA Difference Equations

If the residual errors in (3.7) and (3.8) are white, uncorrelated processes then clearly, consistent estimates from a closed-loop system could possibly result. Now, consider the two following ARMA equations as a possible form of the candidate set of models:

$$y(t) = \sum_{k=1}^{S} g_{1k} y(t-k) + \sum_{k=1}^{R} g_{2k} x(t-k) + W_y(t) \tag{3.9}$$

$$x(t) = \sum_{k=1}^{T} j_{1k} x(t-k) + \sum_{k=1}^{U} j_{2k} y(t-k) + W_x(t) \tag{3.10}$$

where S, R, T, U are all of finite value and $W_y(t)$ and $W_x(t)$ are respectively the residual errors. These residual errors are defined to be white, Gaussian processes that are uncorrelated with each other. At first glance, it seems unlikely that these equations can properly represent the dynamics of the true system, since these equations are different from those of the true system. Additionally, (3.9) and (3.10) must be able to account for the colored residual errors respectively in (3.7) and (3.8). This also seems to be

impossible as the residual errors of (3.9) and (3.10) are white. However, by examining (3.9) and (3.10) more carefully, it turns out that these equations can indeed account for the dynamics of the true system and the colored residual errors. This can best be shown by introducing a linear operator notation.

The forward operator q and the backward operator q^{-1} are introduced as follows:

$$qu(t) = u(t+1)$$

$$q^{-1}u(t) = u(t-1).$$

where $u(t)$ is some discrete-time sequence. Now, (3.9) can be written as follows:

$$y(t) = \sum_{k=1}^{S} g_{1k}(q^{-k}y(t)) + \sum_{k=1}^{R} g_{2k}(q^{-k}x(t)) + W_y(t)$$

$$= \left[\sum_{k=1}^{S} g_{1k}q^{-k}\right]y(t) + \left[\sum_{k=1}^{R} g_{2k}q^{-k}\right]x(t) + W_y(t)$$

$$= G_1(q)y(t) + G_2(q)x(t) + W_y(t)$$

where $G_1(q)$ and $G_2(q)$ are called transfer operators or transfer functions. Solving this equation for $y(t)$ results in

$$y(t) = \frac{G_2(q)}{1-G_1(q)}x(t) + \frac{1}{1-G_1(q)}W_y(t).$$

For comparative purposes, the application of this linear operator notation to the true system in (3.7) results in

$$y(t) = H_1(q)x(t) + N_y(t).$$

Therefore, (3.9) can represent the dynamics of (3.7) provided that

$$\frac{G_2(q)}{1-G_1(q)} = H_1(q) \tag{3.11}$$

$$\frac{1}{1-G_1(q)}W_y(t) = N_y(t). \tag{3.12}$$

The left side of the equality in (3.11) is a finite order ARMA transfer function, while the right side of the equality is an infinite order MA transfer function. This equality is possible because in theory, finite order ARMA transfer functions can be equivalent to infinite order MA transfer functions [30]. Furthermore, (3.12) shows that the colored

residual error of the true system can be accounted for by (3.9) via the AR terms. (3.12) basically shows that a function of the AR terms is to whiten the colored residual error. The left side of the equality in (3.12) is generally referred to as the actual error of an ARMA equation. Equality of (3.11) and (3.12) requires that the proper parameterization is chosen. Therefore, the ARMA equation in (3.9) can equivalently represent the dynamics of the true system and the colored residual error. Additionally, its residual error is white and uncorrelated with the residual error of (3.8). By using some of the methods that will be presented in Section 3.4.2, it is not difficult to show that the least squares estimation of (3.9) results in consistent parameter estimates. Of course, all these results apply to (3.10) as well.

3.3.3 Simulation Experiments

To further demonstrate the concept that a closed-loop system whose open-loop couplings are described by MA equations with colored noise can be estimated better with ARMA equations than MA equations, simulation experiments were performed using the closed-loop system in Figure 3-6. The open-loop coupling H_1 was described by the following MA equation:

$$y(t) = \sum_{k=1}^{99} -(.95)^{k-1} x(t-k) + N_y(t) \tag{3.13}$$

where $N_y(t)$ is colored noise. Figures 3-7a and 3-8a respectively show the actual impulse response of H_1 and the actual power spectrum of $N_y(t)$. The other open-loop coupling H_2 was also described by an MA equation as follows:

$$x(t) = \sum_{k=1}^{99} (-.9)^{k-1} y(t-k) + N_x(t) \tag{3.14}$$

where $N_x(t)$ is colored noise as well. Figures 3-7a and 3-8a also respectively show the actual impulse response of H_2 and the actual power spectrum of $N_x(t)$. The input-output data $x(t)$ and $y(t)$ was generated using (3.13) and (3.14) and $N_y(t)$ and $N_x(t)$.

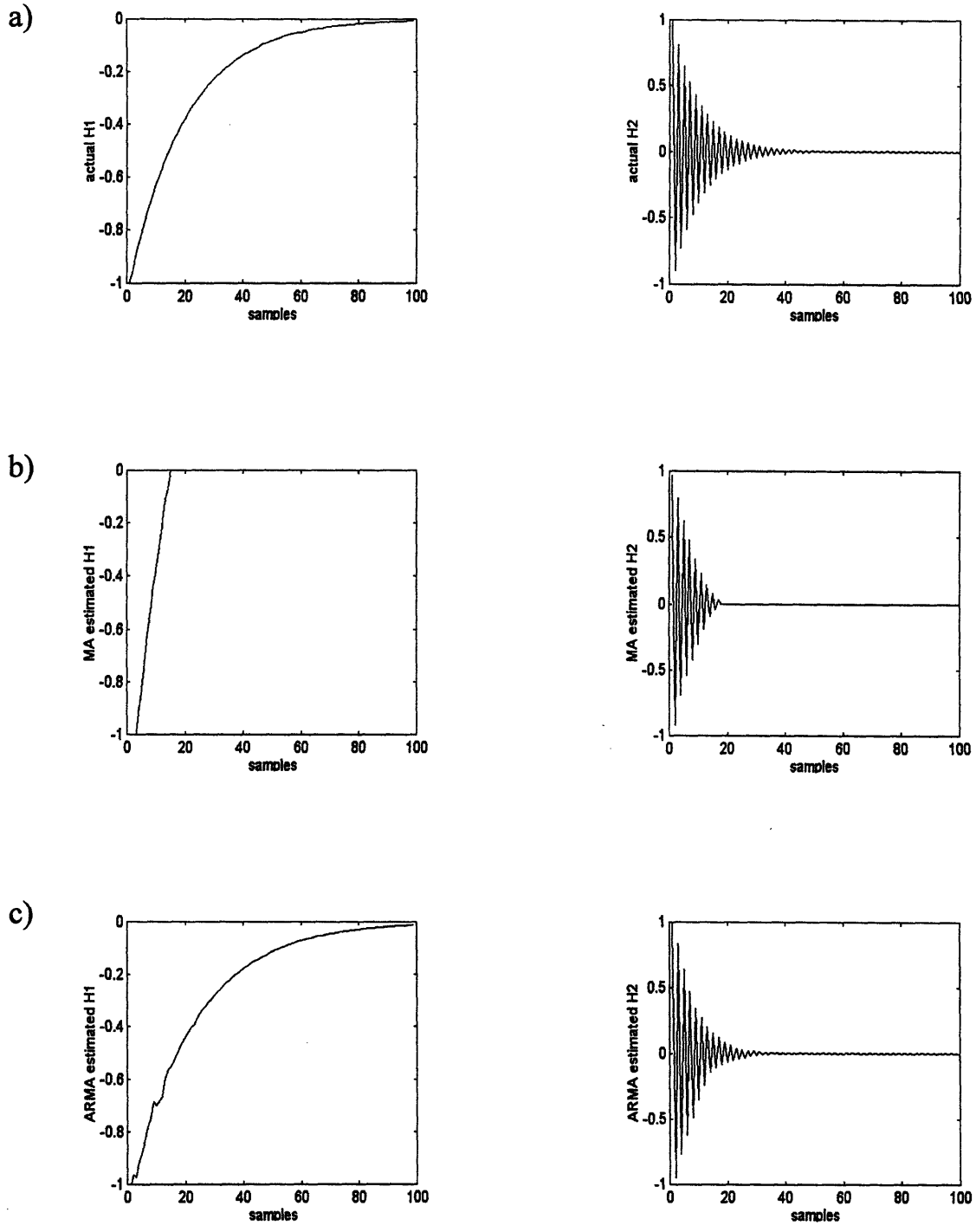

Figure 3-7: a) Actual impulse responses of H_1 and H_2 in the simulated closed-loop system. b) Estimated impulse responses for H_1 and H_2 resulting from MA equations. c) Estimated impulse responses for H_1 and H_2 resulting from ARMA equations.

a)

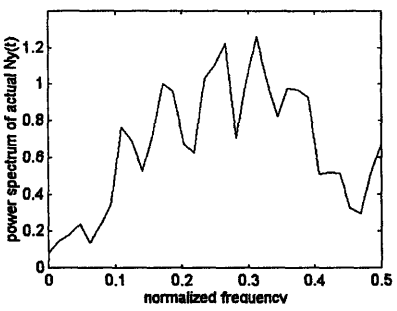

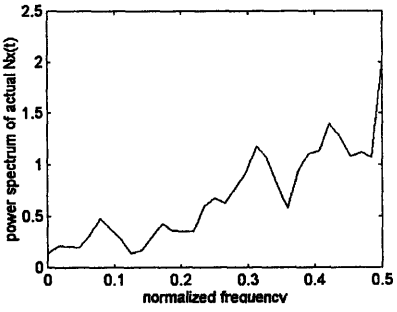

b)

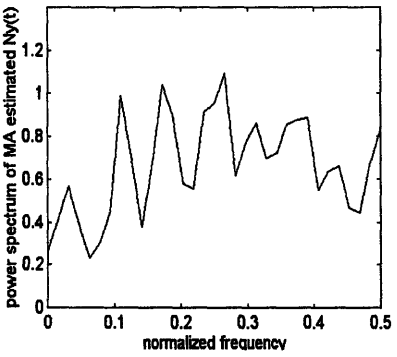

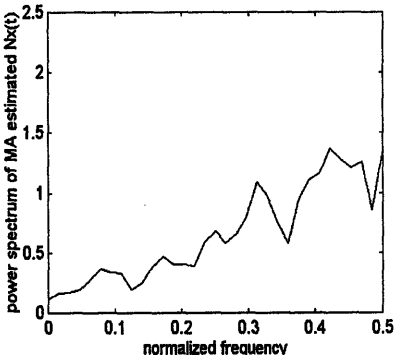

c)

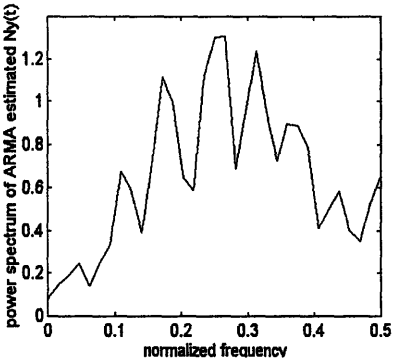

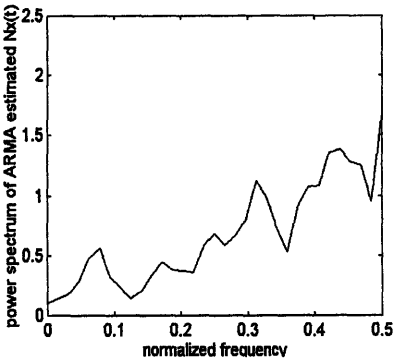

Figure 3-8: a) Actual power spectra of $N_y(t)$ and $N_x(t)$ in the simulated closed-loop system. b) Estimated power spectra for $N_y(t)$ and $N_x(t)$ resulting from MA equations. c) Estimated power spectra for $N_y(t)$ and $N_x(t)$ resulting from ARMA equations.

The form of the candidate set of models was first chosen to be MA as in (3.7) and (3.8). The set of different parameterizations was chosen in conjunction with Akaike's Final Prediction Error (FPE) information criterion which is as follows:

$$FPE(n) = \frac{1 + n/N}{1 - n/N} * V_n$$

where n is the number of parameters, N is the number of samples of data, and V_n is the loss function computed from n parameters. As discussed in Section 2.1.3., the FPE essentially chooses a parameterization by penalizing the loss function with the number of parameters. Therefore, by minimizing the FPE, a parameterization is chosen that sufficiently describes the dynamics of the system in question without overparameterization. N is also included in the FPE because, in theory, the larger N is, the better the estimate should be. Therefore, N allows for the comparison of models that are generated from different data lengths. However, the data lengths were constant in this simulation, so N is not a factor. Of course, in this case, V_n was determined via least squares estimation.

The choice of the "best" model was determined from the generated data by first choosing the parameterization. This was done as follows: The order of the difference equation (P or Q) was initially set to one and then incremented by one and each time the FPE was computed. Each time, the FPE should decrease until overparameterization occurs, and then the FPE should begin to increase. The parameterization that produced the minimum FPE was chosen and least squares was applied to this difference equation to estimate the parameters. Of course, least squares must be applied to the entire set of parameterizations as V_n is required for the computation of the FPE. Figures 3-7b and 3-8b respectively show the resulting MA estimated impulse response of H_1 and the MA estimated power spectrum of $N_y(t)$. Figures 3-7b and 3-8b also respectively show the resulting MA estimated impulse response of H_2 and the MA estimated power spectrum of $N_x(t)$.

Next, the form of the difference equations was chosen to be ARMA as in (3.9) and (3.10). The same incremental procedure used for the MA equations was applied to

estimate these parameters except this time the number of AR and MA parameters were stepped up in tandem beginning with one AR parameter and one MA parameter. Figures 3-7c and 3-8c respectively show the resulting ARMA estimated impulse response of H_1 and the ARMA estimated power spectrum of $N_y(t)$. Figures 3-7c and 3-8c also respectively show the resulting ARMA estimated impulse response of H_2 and the ARMA estimated power spectrum of $N_x(t)$. As discussed in the previous section, the ARMA estimated $N_y(t)$ and $N_x(t)$ are actual errors and not residual errors. It is obvious from Figures 3-7 and 3-8 that estimation with ARMA equations provided a better representation of the true closed-loop system than estimation with MA equations just as theory predicted. However, more formally, the normalized mean-squared error (NMSE) was calculated for the MA estimated residual errors and for the ARMA estimated actual errors. The NMSE in this case is defined to be

$$NMSE = \frac{Var(N_{actual}(t) - N_{estimated}(t))}{Var(N_{actual}(t))}$$

where $Var(\cdot)$ is the variance operator. The NMSE's for the MA estimated $N_y(t)$ and $N_x(t)$ are respectively 0.085 and 0.035. On the other hand, the NMSE's for the ARMA estimated $N_y(t)$ and $N_x(t)$ are respectively 0.018 and 0.023. These results further support the use of ARMA equations in estimating closed-loop systems with colored residual errors.

So the form of the difference equations that describe the dynamics of the closed-loop model of short-term cardiovascular control in Figure 3-3 is selected to be

$$HR(t) = \sum_{k=1}^{Q} a_k HR(t-k) + \sum_{k=1}^{R} d_{1k} ABP(t-k) + \sum_{k=S'}^{S} d_{2k} ILV(t-k) + W_{HR}(t) \quad (3.15)$$

$$ABP(t) = \sum_{k=1}^{T} f_k ABP(t-k) + \sum_{k=1}^{U} g_{1k} IHR(t-k) + \sum_{k=V'}^{V} g_{2k} ILV(t-k) + W_{ABP}(t) \quad (3.16)$$

where $W_{HR}(t)$ and $W_{ABP}(t)$ are the residual errors. These residual errors are defined to be white, Gaussian processes with variances σ^2_{HR} and σ^2_{ABP} that are uncorrelated with each other. The set of parameterizations for (3.15) and (3.16) now needs to be chosen. This issue will be discussed in conjunction with the determination of the "best" parameterization in Section 3.4.1.

3.4 Determination of the "Best" Model in the Set

Now that a candidate set of models has been nearly chosen, the next step in the general system identification procedure is to determine the "best" model in this set based on the input-output data. First, the "best" parameterization must be determined which is normally accomplished by minimizing some information criterion. As discussed in Sections 2.1.3 and 3.3.3, information criteria typically penalize the loss function with the number of parameters of the model in order to avoid both underparameterization and overparameterization. Once a parameterization is chosen, an identification method, specifically least squares in this thesis, can then be applied to estimate the "best" parameters of the difference equation. The loss function can only be computed via the residual error resulting from least squares estimation. Therefore, least squares plays a major role in the determination of the parameterization as well. Of course, it is essential that the resulting estimates are consistent i.e., the system is identifiable.

3.4.1 Least Squares Estimation and the APR Algorithm

The parameters of each difference equation in (3.15) and (3.16) are estimated separately. From Section 3.1.2, (3.15) is to be estimated with 1.5 Hz data, while (3.16) is to be estimated with 90 Hz data. Since the fundamentals of least squares estimation were presented in Section 3.2, only the least squares solution is shown here. In particular, the least squares solution for (3.15) is

$$\hat{\theta} = (\Phi^{\mathrm{T}}\Phi)^{-1}\Phi^{\mathrm{T}} HR \tag{3.17}$$

where

$$\hat{\theta}^{\mathrm{T}} = [a_1 \cdots a_Q \quad d_{11} \cdots d_{1R} \quad d_{2S'} \cdots d_{2S}]$$

$$HR^{\mathrm{T}} = [HR(t)\ HR(t+1) \cdots HR(t+N-1)]$$

$$\Phi^{\mathrm{T}} = [\phi(t)\ \phi(t+1) \cdots \phi(t+N-1)]$$

and

$$\phi^{\mathrm{T}}(t) = [HR(t-1) \cdots HR(t-Q) \quad ABP(t-1) \cdots ABP(t-R) \quad ILV(t-S') \cdots ILV(t-S)].$$

Note that N denotes the number of equations in the least squares problem. The least squares estimate resulting from (3.16) can be similarly shown.

However, before least squares can be implemented, a set of parameterizations must be selected. The set of parameterizations is chosen with an ARMA parameter reduction (APR) algorithm. This algorithm also determines the "best" parameterization from the chosen set of parameterizations with the aid of the Rissanen's minimum description length (MDL) criterion which is as follows:

$$MDL(n) = \left(1 + n\frac{\log(N)}{N}\right)\frac{V_n}{N}$$

where n is the number of parameters of the difference equation, N is the number of data samples, and V_n is the loss function computed when the difference equation consists of n parameters. The loss function is determined by calculating the mean-squared residual error resulting from least squares estimation. The rationale for the terms n, N, and V_n in the MDL value is essentially the same as that discussed in Section 3.3.3 for these terms in the FPE value. A detailed discussion of information criteria is in [28,39].

A complete treatment of the APR algorithm can be found in [34]; however, its essentials are summarized here. This algorithm is based on determining the parameterization from a "maximal model." The maximal model is an overparameterized model that is assumed to include the true parameterization. The idea is that the parameters estimated from the maximal model are more likely to be true parameters if they are of large magnitudes. However, it can be shown that each parameter estimate is corrupted by different levels of noise. So, more precisely, an estimated parameter is more likely to be a true parameter if its magnitude is large relative to its corresponding noise level i.e., it has a large signal to noise ratio (SNR).

It should be noted that the AR parameters are treated separately from the MA parameters. One reason for this deals with changes in gain between the input and output. In this situation, the parameterization is still the same; however, the SNR of the MA parameters change, while the SNR of AR parameters remain the same. This will result in either a bias towards MA parameters or AR parameters depending on the exact change in gain. Clearly, the parameterization selection procedure should be insensitive to the

relative gain between the input and output. Another point to note is that many biological systems tend to have delays in their MA parameters but not in their AR parameters. The concept of such delays is best understood with an example. Consider a difference equation whose MA parameters are b_k where $k \in [1,50]$. All the b_k's that are zero in this range are the delays. These delays have no effect on the loss function but are still considered to be parameters of the difference equation. Therefore, delays cause the MDL value to be higher than it really should be. If the delays are not included in the parameterization, the MDL value will be determined appropriately. However, since the delays are unknown, this implies that there are much more than just 50 possible parameterizations and to search through all these parameterizations would be intractable. In fact, this is the advantage of the APR algorithm which gets around this problem via the SNR technique. However, the SNR technique is only necessary to determine the MA parameterization, since the AR parameters do not have the problem of delays.

Based on the aforementioned information, the procedure for the determination of the "best" model is as follows:

1) A maximal model that is believed to include the true parameterization is selected. Based on experience, the maximal models are chosen for (3.15) to be $Q=10$, $R=15$, $S'=-10$, and $S=15$ and for (3.16) to be $T=10$, $U=35$, $V'=0$, and $V=15$.

2) The AR parameters are decreased one at a time beginning with the AR parameter of largest lag, thus creating "reduced models."

3) The reduced model with the smallest MDL value is chosen as the proper reduced model and so the AR parameterization is determined.

4) The SNR for each MA parameter of the reduced model is computed.

5) The MA parameters are removed one at a time beginning with the MA parameter with the lowest SNR, hence creating "minimal models."

6) The minimal model with the smallest MDL value is chosen as the proper minimal model and so the MA parameterization is determined.

7) Least squares is then applied to estimate the parameters of this minimal model.

3.4.2 Consistency of the Parameter Estimates

It is of paramount importance that the least squares estimation of the parameters in the ARMA equations in (3.15) and (3.16) result in consistent estimates. The task that is undertaken here is to show that this is indeed the case. From Section 3.2.4, the conditions for consistent least squares estimation are that 1) $E(\phi(t)\phi^{T}(t))$ is nonsingular and 2) $E(\phi(t)e(t)) = 0$. Consistency will be shown only for the least squares estimates resulting from (3.15). However, the methods that are presented here can be used to show the consistency for the least squares estimates resulting from (3.16) as well.

Before the nonsingularity condition can be shown to hold, a few pertinent results in linear algebra must be presented. A symmetric matrix A is positive semidefinite ($A \geq 0$) if

$$x^{T}Ax \geq 0$$

for all vectors x. This matrix A is positive definite ($A > 0$) if

$$x^{T}Ax > 0$$

for all vectors $x \neq 0$. The sum of a positive semidefinite matrix A and a positive definite matrix B results in a positive definite matrix since

$$x^{T}(A+B)x = x^{T}Ax + x^{T}Bx > 0.$$

It is not difficult to see that a positive semidefinite matrix is positive definite if and only if it is invertible or nonsingular. Nonsingular matrices have a full set of linearly independent columns. The number of linearly independent columns of a matrix is referred to as the rank of the matrix. Therefore, a nonsingular matrix has full rank. A more complete treatment of these concepts can be found in [40].

Now, the nonsingularity condition is shown to hold via a simplification, two matrix results, and the concept of persistent excitation. For simplicity, (3.15) and (3.16) can be rewritten as follows:

$$HR(t) = x(t) + W_{HR}(t)$$

$$ABP(t) = y(t) + W_{ABP}(t)$$

where

$$x(t)=\sum_{k=1}^{Q} a_k HR(t-k)+\sum_{k=1}^{R} d_{1k} ABP(t-k)+\sum_{k=S'}^{S} d_{2k} ILV(t-k)$$

$$y(t)=\sum_{k=1}^{T} f_k ABP(t-k)+\sum_{k=1}^{U} g_{1k} IHR(t-k)+\sum_{k=V'}^{V} g_{2k} ILV(t-k).$$

This simplification is similar to that found in [43]. Now, from this simplification and $\phi(t)$ in (3.17),

$$E(\phi(t)\phi^{\mathrm{T}}(t))=\begin{array}{c} \\ Q \\ R \\ S'' \end{array}\begin{array}{c} \begin{array}{ccc} Q & R & S'' \end{array} \\ \begin{bmatrix} R_x & R_{xy} & R_{xILV} \\ R_{yx} & R_y & R_{xABP} \\ R_{ILVx} & R_{ABPx} & R_{ILV} \end{bmatrix} \end{array}+\begin{bmatrix} \sigma_{HR}^2 I & 0 & 0 \\ 0 & \sigma_{ABP}^2 I & 0 \\ 0 & 0 & 0 \end{bmatrix} \tag{3.18}$$

where the elements of the left-sided matrix are all covariance matrices and Q, R, and $S''=S-S'+1$ represent the dimensions of these matrices. For example, R_{xABP} is a cross-covariance matrix with R rows and S'' columns. Of course, by definition, the left-sided matrix is also a covariance matrix with $Q+R+S''$ rows and columns. Two properties that characterize all covariance matrices are that they are symmetric and positive semidefinite and possibly positive definite. (3.18) can be rewritten as follows:

$$E(\phi(t)\phi^{\mathrm{T}}(t))=\begin{array}{c} \\ P \\ S'' \end{array}\begin{array}{c} \begin{array}{cc} P & S'' \end{array} \\ \begin{bmatrix} A' & B \\ B^{\mathrm{T}} & C \end{bmatrix} \end{array}+\begin{bmatrix} A'' & 0 \\ 0 & 0 \end{bmatrix} \tag{3.19}$$

where

$$A'=\begin{bmatrix} R_x & R_{xy} \\ R_{yx} & R_y \end{bmatrix} \qquad B=\begin{bmatrix} R_{xILV} \\ R_{xABP} \end{bmatrix} \qquad C=R_{ILV} \qquad A''=\begin{bmatrix} \sigma_{HR}^2 I & 0 \\ 0 & \sigma_{ABP}^2 I \end{bmatrix}$$

and $P = Q+R$. A'' is positive definite since it is the covariance matrix of the vector

$$\begin{bmatrix} W_{HR}(t-1)\cdots W_{HR}(t-Q) & W_{ABP}(t-1)\cdots W_{ABP}(t-R) \end{bmatrix}^{\mathrm{T}}$$

and it is nonsingular. Of course, the left-sided matrix in (3.19) is still positive semidefinite as it has not changed. By additionally assuming that C is positive definite, then the following two matrix results apply:

$$A' - BC^{-1}B^{\mathrm{T}} \geq 0$$

and

$$rank\ E(\phi(t)\phi^{\mathrm{T}}(t)) = S'' + rank\ (A'' + A' - BC^{-1}B^{\mathrm{T}}).$$

The derivation of these two matrix results can be found in [39]. Since the sum of a positive definite matrix and a positive semidefinite matrix always results in a positive definite matrix and a positive definite matrix always has full rank,

$$rank\ (A'' + A' - BC^{-1}B^{\mathrm{T}}) = P$$

and so

$$rank\ E(\phi(t)\phi^{\mathrm{T}}(t)) = (S - S' + 1) + Q + R.$$

This equation means that the covariance matrix $E(\phi(t)\phi^{\mathrm{T}}(t))$ has full rank which implies nonsingularity.

All that is left is to show that C which is R_{ILV} is positive definite and so, the concept of persistent excitation is now formally introduced. This treatment is essentially that in [28]. A stationary signal $u(t)$ with power spectrum $S_u(\omega)$ is defined to be persistently exciting of order n, if for all filters of the form

$$M_n(z) = m_1 z^{-1} + \cdots + m_n z^{-n},$$

the relation

$$\left|M_n(e^{j\omega})\right|^2 S_u(\omega) \equiv 0 \text{ implies that } M_n(e^{j\omega}) \equiv 0. \tag{3.20}$$

This definition can be interpreted in a more meaningful way. Note that

$$\left|M_n(e^{j\omega})\right|^2 = M_n(z)M_n(z^{-1})\big|_{z=e^{j\omega}},$$

that is, provided that the inverse z-transform of $M_n(z)$ is real. $M_n(z)M_n(z^{-1})$ must always have one zero at the origin of the z-plane and any zero on the unit circle of the z-plane or equivalently, the ω-axis, must also be accompanied by a duplicate zero. Therefore, $\left|M_n(e^{j\omega})\right|^2$ can potentially be zero for at most $n-1$ different values of ω and so, $u(t)$ is persistently exciting of order n if $S_u(\omega)$ is different from zero at at least n different values of ω.

Now, consider the vector

$$u^{\mathrm{T}} = [u(t)\ u(t+1)\cdots u(t+n-1)].$$

Let the covariance matrix of this vector be R_u. If $u(t)$ is persistently exciting of order n, then R_u is positive definite. The proof follows. By definition, R_u is positive definite if

$$m^{\mathrm{T}} R_u m = 0 \Rightarrow m = 0.$$

It can be shown that

$$m^{\mathrm{T}} R_u m = E\{(M_n(q)u(t))^2\}$$

where the linear operator notation introduced in Section 3.3.2 is used. Therefore, from [38],

$$m^{\mathrm{T}} R_u m = \frac{1}{2\pi}\int_{-\pi}^{\pi} \left|M_n(e^{j\omega})\right|^2 S_u(\omega)d\omega\ .$$

Since $u(t)$ is persistently exciting of order n, (3.20) applies. Hence, this integral is zero only when

$$M_n(e^{j\omega}) \equiv 0$$

which implies that

$$m^{\mathrm{T}} R_u m = 0 \text{ only when } m = 0\ .$$

So, if $ILV(t)$ is persistently exciting of at least order $S\text{-}S'+1$, the covariance matrix of $ILV(t)$ or R_{ILV} is positive definite. The power spectrum of $ILV(t)$ is broadband as a result of the random-interval breathing technique. This technique produces many more non-zero values of the power spectrum of $ILV(t)$ than 26 which is the maximum value of $S\text{-}S'+1$ (see Section 3.4.1). Therefore, the covariance matrix R_{ILV} is positive definite and so the nonsingularity condition is satisfied.

Now the second condition for consistency is shown to hold. This condition requires that

$$E(\phi(t)W_{HR}(t)) = E\begin{bmatrix} HR(t-1)W_{HR}(t) \\ \vdots \\ HR(t-Q)W_{HR}(t) \\ ABP(t-1)W_{HR}(t) \\ \vdots \\ ABP(t-R)W_{HR}(t) \\ ILV(t-S')W_{HR}(t) \\ \vdots \\ ILV(t-S)W_{HR}(t) \end{bmatrix} = 0. \qquad (3.21)$$

Because (3.15) is strictly causal and $W_{HR}(t)$ is a white process, the first Q elements of (3.21) are clearly zero. As mentioned in section 3.3.1, the sinoatrial node is causal and so, $IHR(t)$ depends on only the past and present values of the $\{HR(t)\}$ sequence. Therefore, from (3.16), the middle R elements of $\phi(t)$ contain contributions from the past values of the $\{HR(t)\}$ sequence and thus the past values of the $\{W_{HR}(t)\}$ sequence (closed-loop is strictly causal). These contributions maybe nonlinear, but they are still uncorrelated with $W_{HR}(t)$ which is white. Therefore, the middle R elements of (3.21) are also zero. Finally, the last S-S'+1 elements of this vector are zero as $W_{HR}(t)$ is white and thus, uncorrelated with the sequence $\{ILV(t)\}$. It should be noted that white residual errors and a strictly causal closed-loop are sufficient features for this condition to hold. Since it has been shown that these two features do apply here, consistent parameter estimates will be obtained.

3.4.3 System Identification of ILV→ABP

The ultimate goal of the closed-loop system identification procedure is not to estimate the parameters of (3.15) and (3.16) but to estimate the transfer relations and noise perturbations in the closed-loop model of short-term cardiovascular control mechanisms. These transfer relations are implicit in the ARMA difference equations of (3.15) and (3.16). They can be made explicit via the z-transform which is defined as follows:

$$H(z) = \sum_{k} h(k)z^{-k}$$

where $h(t)$ is some discrete-time sequence. Consider the z-transform of (3.16) as follows:

$$ABP(z) = \frac{\sum_{k=1}^{U} g_{1k} z^{-k}}{1 - \sum_{k=1}^{Q} f_k z^{-k}} IHR(z) + \frac{\sum_{k=V'}^{V} g_{2k} z^{-k}}{1 - \sum_{k=1}^{Q} f_k z^{-k}} ILV(z) + \frac{1}{1 - \sum_{k=1}^{Q} f_k z^{-k}} W_{ABP}(z).$$

From this equation, the CIRCULATORY MECHANICS transfer relation is defined to be

$$\frac{ABP(z)}{IHR(z)} = \frac{\sum_{k=1}^{U} g_{1k} z^{-k}}{1 - \sum_{k=1}^{Q} f_k z^{-k}},$$

while the ILV→ABP transfer relation is defined to be

$$\frac{ABP(z)}{ILV(z)} = \frac{\sum_{k=V'}^{V} g_{2k} z^{-k}}{1 - \sum_{k=1}^{Q} f_k z^{-k}}. \tag{3.22}$$

Clearly, the parameter estimates are essential to the goal of this thesis as they are necessary to estimate the transfer relations. Of course, the z-transform can be similarly applied to (3.15).

The estimation of the parameters of (3.16) is accomplished with 90 Hz input-output data to accommodate the spectral content of the ABP waveform. From (3.22), this means that ILV→ABP is also estimated with 90 Hz data. However, the data required to estimate this transfer relation need only be sampled at 1.5 Hz as this will be more than sufficient for the spectral content of ILV. The 90 Hz ILV data contains only noise above about 0.5 Hz, and this noise may corrupt the parameter estimates. Therefore, it is appropriate to estimate this transfer relation at 1.5 Hz. The system identification procedure to perform this estimation is presented here.

As in any system identification procedure, the first step is to generate the input-output data. This is done in two steps. In the first step, the IHR data is fed through the estimated model resulting from (3.16) with ILV set to zero, thus creating the portion of ABP which is only attributable to IHR. This data is referred to as ABP_{IHR}. ABP_{IHR} is then subtracted from the 90 Hz ABP data, creating the portion of ABP that is attributable

to ILV and noise. This data is called $ABP_{IHR'}$. In the next step, $ABP_{IHR'}$ and ILV are decimated to 1.5 Hz. Of course, the next step of the system identification procedure is to select a candidate set of models. The form of the difference equation that is chosen is as follows:

$$ABP_{IHR'}(t) = \sum_{k=1}^{L} h_k ABP_{IHR'}(t-k) + \sum_{k=0}^{M} j_k ILV(t-k) + W'_{ABP}(t) \qquad (3.23)$$

where $W'_{ABP}(t)$ is a white, Gaussian noise process. One may wonder why a MA difference equation is not chosen as ILV→ABP is an open-loop coupling. The reason is that an infinite order MA difference equation would be required which is not computationally feasible. Furthermore, as mentioned previously, a finite order ARMA equation can be equivalent to an infinite order MA difference equation. The parameters are determined using the exact procedure in 3.4.1. Experience shows that the maximal model with *L=10* and *M=15* is very reasonable. From the methods used in Section 3.4.2, it is easy to show that the resulting parameter estimates are consistent. It should be noted that the noise perturbations N_{HR} and N_{ABP} in the closed-loop model respectively refer to the actual error estimated from (3.15) and the actual error estimated from (3.23). At last, the "best" model in the set is determined.

3.5 Validation of the "Best" Model

In the previous three steps of the closed-loop system identification procedure, a "best" model is determined based on the least squares and MDL criterion from a set of candidate models and input-output data. The question that must be dealt with now is as follows: is this "best" model good enough? This is the problem of model validation, and it is the final step in the general system identification procedure. There are several different approaches to deal with this question. Two of these approaches are employed here. The first approach analyzes the residual errors, while the second approach involves the use of *a priori* information about the true system. Normally, if the "best" model is not validated, then steps 1, 2, and/or 3 of the general system identification procedure must be adjusted and the procedure should be repeated again until the "best" model is

validated. However, the goal of the closed-loop system identification procedure is to assess diabetic autonomic neuropathy. Clearly, it would be desirable for the assessment method to be standardized. Therefore, the system identification procedure in this thesis is not iterative and invalid models are considered to be outliers. Since this method generally produces models that are validated, this lack of iteration does not present a major problem.

3.5.1 Residual Error Analysis

The residual errors in (3.15), (3.16), and (3.23) that result from least squares estimation are defined to be white noise processes. If these residual errors are not white, then inconsistent estimation will result. Consequently, the "best" model will be in doubt. However, if the residual errors are white, consistent estimation of the parameters will result. Furthermore, there will be an increased confidence in the chosen AR parameterization, because the AR parameters successfully whitened the colored residual error of the "true" system (see (3.12)). Therefore, it is essential to test the whiteness of the residual errors. In particular, whiteness tests are performed by estimating the unbiased autocorrelation function of the residual errors as follows:

$$R_x(m) = \frac{1}{N-|m|} \sum_{n=0}^{N-|m|-1} x(n)x(n+m)$$

where N is the number of data samples of a residual error sequence $x(t)$. Figures 3-9a, b, and c respectively show the autocorrelation function for lags up to 25 ($m=25$) for $W_{HR}(t)$, $W_{ABP}(t)$, and $W'_{ABP}(t)$ estimated from a typical control subject in the tilted posture. The autocorrelation function of a white noise process is defined to be

$$R_x(m) = \sigma_x^2 \delta(m)$$

where σ_x^2 is the variance of $x(t)$ and $\delta(t)$ is the Dirac delta function. Therefore, these residual errors appear to be sufficiently white.

Unfortunately, this test does not provide an absolute validation of the model because whiteness does not guarantee that the parameterization was chosen appropriately. This may include the AR parameterization as well, since there are many AR

parameterizations that could sufficiently whiten the colored residual error of the "true" system. However, the power of this test is evinced when the whiteness test fails. In this case, inconsistent estimation occurs and hence, the model cannot be validated and is thus rendered an outlier.

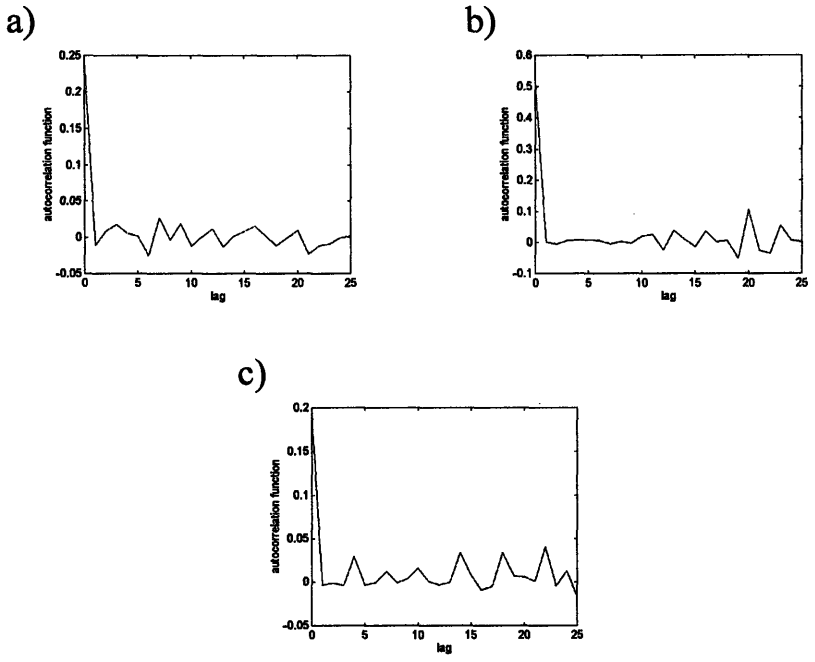

Figure 3-9: The unbiased autocorrelation functions for lags up to 25 of the residual errors as a) $W_{HR}(t)$, b) $W_{ABP}(t)$, and c) $W'_{ABP}(t)$ estimated from a typical control subject in the tilted posture.

3.5.2 *A Priori* Information

The most powerful way to validate the "best" model would be to verify that the model represents the exact dynamics of the true system. Of course, this is impossible because the exact dynamics of the true system are unknown. (If they were known, system identification, and this thesis for that matter, would be unnecessary.) However, some *a priori* information about the cardiovascular control mechanisms is known (see Sections

2.2 and 2.4), and this can be used to at least determine whether the estimates are physiologically reasonable.

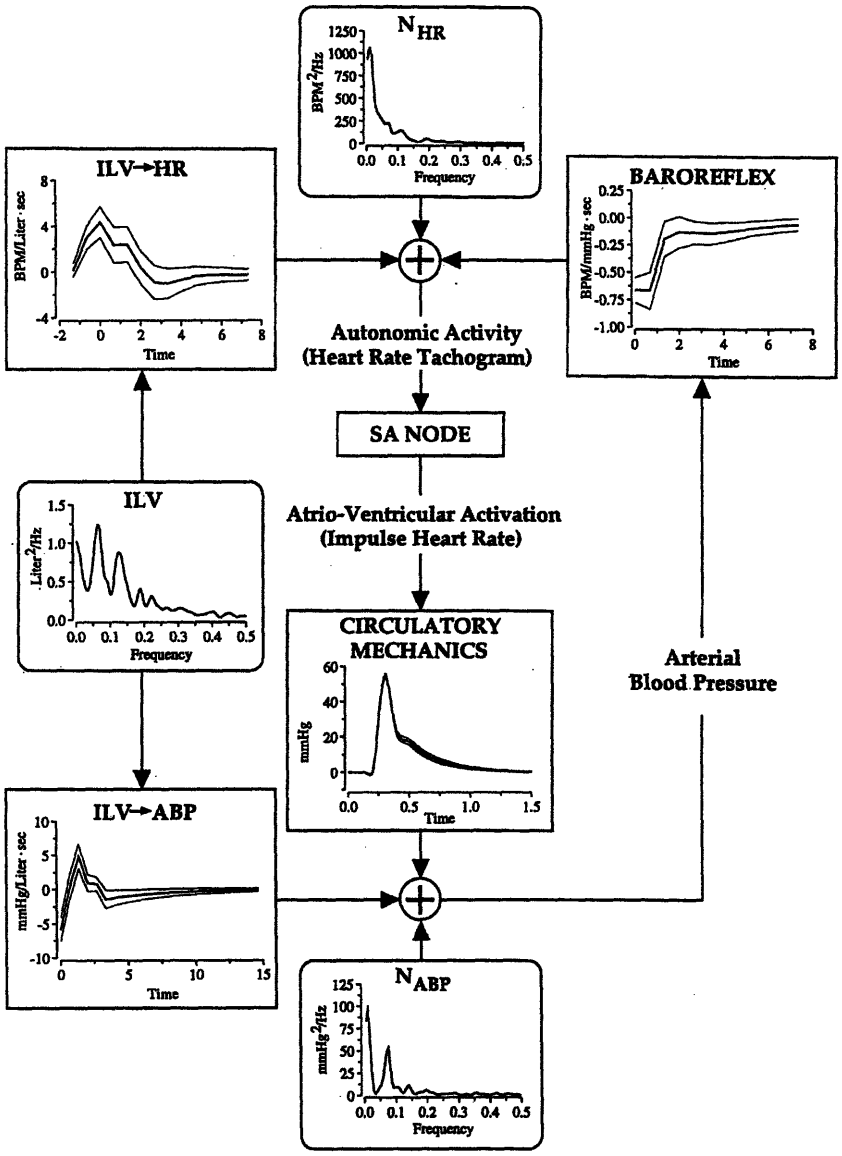

Figure 3-10: Closed-loop model estimates obtained from a typical control subject in the supine posture. The transfer relation estimates are in the form of impulse responses with 95% confidence intervals, while the noise perturbation estimates and ILV are in the form of power spectra.

Figure 3-10 shows the estimates of the transfer relations and noise perturbations in the closed-loop model of short-term cardiovascular control mechanisms obtained from a typical control subject in the supine posture. The transfer relation estimates are shown in the form of impulse responses with 95% confidence intervals. The calculation of the impulse responses with the 95% confidence intervals can be found in [34]. The noise perturbation estimates are shown in the form of power spectra which are computed via the windowed periodogram method with a Gaussian window.

The ILV→HR impulse response estimate shows that for a transient increase in ILV at time zero, HR increases and then returns to baseline. Note that the increase in HR precedes the increase in ILV. This may indicate central nervous involvement as inspiration is anticipated. These findings are in accord with the current understanding of RSA. The BAROREFLEX impulse response estimate implies that HR decreases and then returns to baseline when there is a transient increase in ABP. This appropriately describes the regulatory effect of the baroreceptor reflex. The ILV→ABP impulse response estimate shows that an impulse of ILV causes an immediate drop in ABP followed by an overshoot and then a return to baseline. This result is physiologically reasonable. The immediate drop in ABP is caused by the negative intrathoracic pressure induced by inspiration. The overshoot of ABP results as venous return increases during inspiration which causes an increase in ventricular filling and ABP. ABP's return to baseline occurs because the inspiratory/expiratory effects of the impulse of ILV wear off. The CIRCULATORY MECHANICS impulse response estimate shows that a single ventricular contraction does indeed produce an ABP waveform. The power spectrum of N_{HR} shows that the fluctuations in ILV and ABP do not completely account for HR fluctuations below 0.1 Hz. The power spectrum of N_{ABP} shows that the fluctuations in IHR and ILV do not explain all the variability in ABP fluctuations less than 0.15 Hz. The fact that these couplings do not completely account for the fluctuations in HR and ABP at low frequencies is reasonable, because there are many other physiological variables that are known to impinge on HR and ABP at such frequencies. Note that the power spectrum of ILV is indeed broadband.

Therefore, all of these estimates are consistent with the established physiological principles of the cardiovascular control mechanisms. Clearly, this fact provides powerful support for the validity of the "best" model. Of course, if the estimates are not physiologically reasonable, the model is rendered invalid and is considered an outlier. Finally, the closed-loop system identification procedure is complete.

Chapter 4

Closed-Loop System Identification Applied to Diabetic Autonomic Neuropathy

This chapter presents the application of the closed-loop system identification procedure described in the previous chapter to the study of diabetic autonomic neuropathy. Specifically, details of the materials and methods involved in the study are described and the results, discussion, and conclusion follow.

4.1 Materials and Methods

This section includes a description of the subjects, experimental protocol, data analysis, and statistical analysis used in this study.

4.1.1 Subjects

Fifty-nine diabetic subjects (mean±SEM age: 46±2) and 37 control subjects (mean±SEM age: 42±2) participated in this study. Written, informed consent was

obtained from all subjects. There was no significant difference in mean age between the diabetic group and Control group.

The diabetic subjects were divided into three groups based on an equal weighting of a parasympathetic nervous system measure (supine high frequency power of the heart rate power spectrum [1]) and a predominantly sympathetic nervous system measure (systolic blood pressure (SBP) fall in response to passive tilting [16,41]). A parasympathetic score for each diabetic subject was calculated as the difference between the parasympathetic test result for that subject and the mean parasympathetic test result for the Control group normalized by the standard deviation of the parasympathetic test result for the Control group. A sympathetic score for each diabetic subject was computed similarly. Hence, negative parasympathetic and sympathetic scores respectively reflect reduced parasympathetic and sympathetic nervous function. A total autonomic score for each diabetic subject, referred to as the A-score, was determined by averaging his or her parasympathetic and sympathetic scores. Diabetic subjects were divided into approximately three equally sized groups based on their A-scores. Specifically, diabetic subjects with A-scores greater than 0.25 were placed in Group 1, between -1.0 and 0.25, in Group 2, and less than -1.0, in Group 3. Therefore, autonomic neuropathy is considered to progress from Group 1 to Group 2 to Group 3. There was no significant difference in mean age among these three groups and the Control group. These four groups will henceforth be referred to as the diagnostic groups.

4.1.2 Experimental Protocol

The experimental protocol was approved by the Institutional Review Board and carried out at the Autonomic Evaluation Unit both of the New England Deaconess Hospital, Boston, MA. This experimental protocol included performing the SBP fall in response to passive tilting test and collecting the data for closed-loop system identification and heart rate power spectral analysis.

The experimental protocol for the SBP fall in response to passive tilting test is presented first. SBP was measured non-invasively with a Critikon Dinamap Vital Signs Monitor 1846SX/P (Johnson and Johnson, Critikon Inc., Tampa, FL) connected to an

IBM PC AT via an RS232 serial interface board. SBP was first measured for each subject in the supine posture prior to passive tilting to 60° (relative to the supine posture) by an electrically driven tilt table. Following passive tilting, SBP was measured each minute for a five minute period. The difference between the lowest SBP measured during this period and the SBP measured in the supine posture was recorded as the SBP fall to passive tilting.

The experimental protocol for closed-loop system identification was the same as that presented in Section 3.1. The ECG data collected from this protocol is used for heart rate power spectral analysis as well.

4.1.3 Data Analysis

Data analysis included both the calculation of the supine high frequency power of the heart rate power spectrum and closed-loop system identification. The heart rate power spectrum was constructed by applying the windowed periodogram method with a Gaussian window to the heart rate tachogram (HR) introduced in Section 3.1.2. A detailed account of the generation of this HR power spectrum is given in [11]. The power in the frequency band between 0.15 and 0.50 Hz was calculated as the supine high frequency power of the heart rate power spectrum.

Closed-loop system identification has already been discussed in detail in Chapter 3. The impulse response estimates that resulted from closed-loop system identification were characterized with the following three parameters: peak amplitude, area, and characteristic time [4]. Let $h(t)$ represent an impulse response as a function of time. Then, these parameters were calculated as follows:

$$PeakAmplitude = \max(h(t))$$

$$Area = T\sum_{t} h(t)$$

$$CharacteristicTime = \frac{\sum_{t} t|h(t)|}{\sum_{t}|h(t)|}$$

where T is the appropriate sampling period. Since the BAROREFLEX shows a negative HR response to a transient increase in ABP, the peak amplitude of its impulse response estimate was computed as follows:

$$PeakAmplitude = \left|\min(h(t))\right|.$$

The noise perturbation estimates in the form of power spectra (windowed periodogram method with Gaussian window) were characterized with three parameters as well. These parameters were determined by computing the power in the spectra of the noise perturbation estimates in the following three frequency bands: dc to 0.50 Hz (total power), dc to 0.15 Hz (low frequency power), and 0.15 to 0.50 Hz (high frequency power).

4.1.4 Statistical Analysis

Comparison of each parameter of the impulse response and noise perturbation estimates were made across the diagnostic groups using one-way analysis of variance (ANOVA) and multiple comparison (Tukey Honest Significant Difference for Unequal Sample Sizes) tests. The null hypothesis of the ANOVA and multiple comparison tests was that the means of the groups under comparison were the same. The null hypothesis was rejected when $p < 0.05$. Nonparametric, sample-by-sample comparisons of each impulse response and noise perturbation estimate were also performed across the diagnostic groups using one-way ANOVA tests. Impulse response and noise perturbation estimates were considered to be different across the diagnostic groups when the null hypothesis (the means of the groups under comparison were the same) was rejected for at least one sample. Since there were many samples associated with each estimate, many ANOVA tests were performed for the comparison of each estimate across the diagnostic groups. Therefore, to account for these multiple comparisons, the ANOVA significance level α was chosen so that the probability of rejecting the null hypothesis incorrectly at least once during the multiple comparisons α^* was equal to 0.05. This was done as follows:

$$\alpha^* = 1-(1-\alpha^n) \Rightarrow \alpha = 1-(0.95)^{1/n}$$

where n is the number of multiple comparisons. Thus, the null hypothesis was rejected when $p < \alpha$. It should be noted that the statistical tests employed here assume that the data was normally distributed. Log transforming the data is a common statistical technique that often makes the data more normally distributed. This technique worked well here and so, all the parameters were logarithmically transformed. The exceptions were the area parameter and the samples of the impulse response estimates, since they may take on negative values. All statistical calculations were made using the Statistica software package (StatSoft, Inc., Tulsa, OK). A more complete treatment of these statistical techniques can be found in [18].

4.2 Results

The resulting averages of the closed-loop model estimates for the diagnostic groups are shown in Figure 4-1. These averages are a result of data obtained while the subjects were in the tilted posture. The autonomically mediated ILV→HR impulse response is largest for the Control group and then diminishes as autonomic neuropathy progresses across the three diabetic groups. These impulse responses show that for a transient increase in ILV at time zero, HR increases and then returns to baseline. Note that these impulse responses all show that an increase in HR precedes the increase in ILV. This suggests at least some neural involvement in each of the four impulse responses since inspiration is anticipated. The autonomically mediated BAROREFLEX impulse response changes across the diagnostic groups in a similar fashion. These impulse responses show a decrease in HR followed by its return to baseline in response to a transient increase in ABP. This also reflects at least some neural involvement in each of the four impulse responses. The mechanical coupling ILV→ABP impulse response seems to be unchanged across the diagnostic groups. Each impulse response shows that an impulse of ILV causes an immediate drop in ABP followed by an overshoot and then a return to baseline. The primarily mechanical coupling CIRCULATORY MECHANICS impulse response seems to be the same across the diagnostic groups as well. These impulse responses show the ABP waveform resulting from a single ventricular

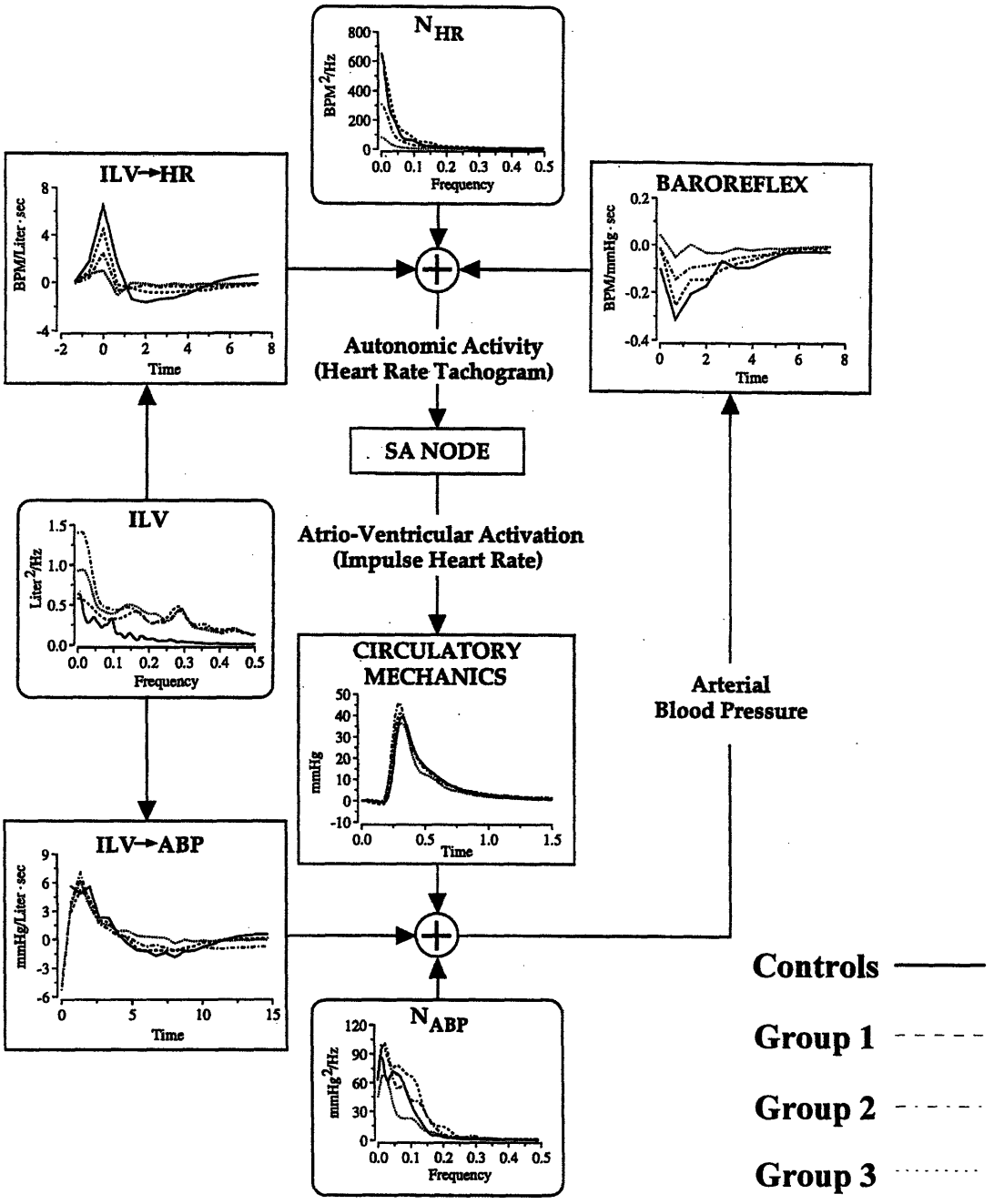

Figure 4-1: The averages of the closed-loop model estimates for the diagnostic groups in the tilted posture.

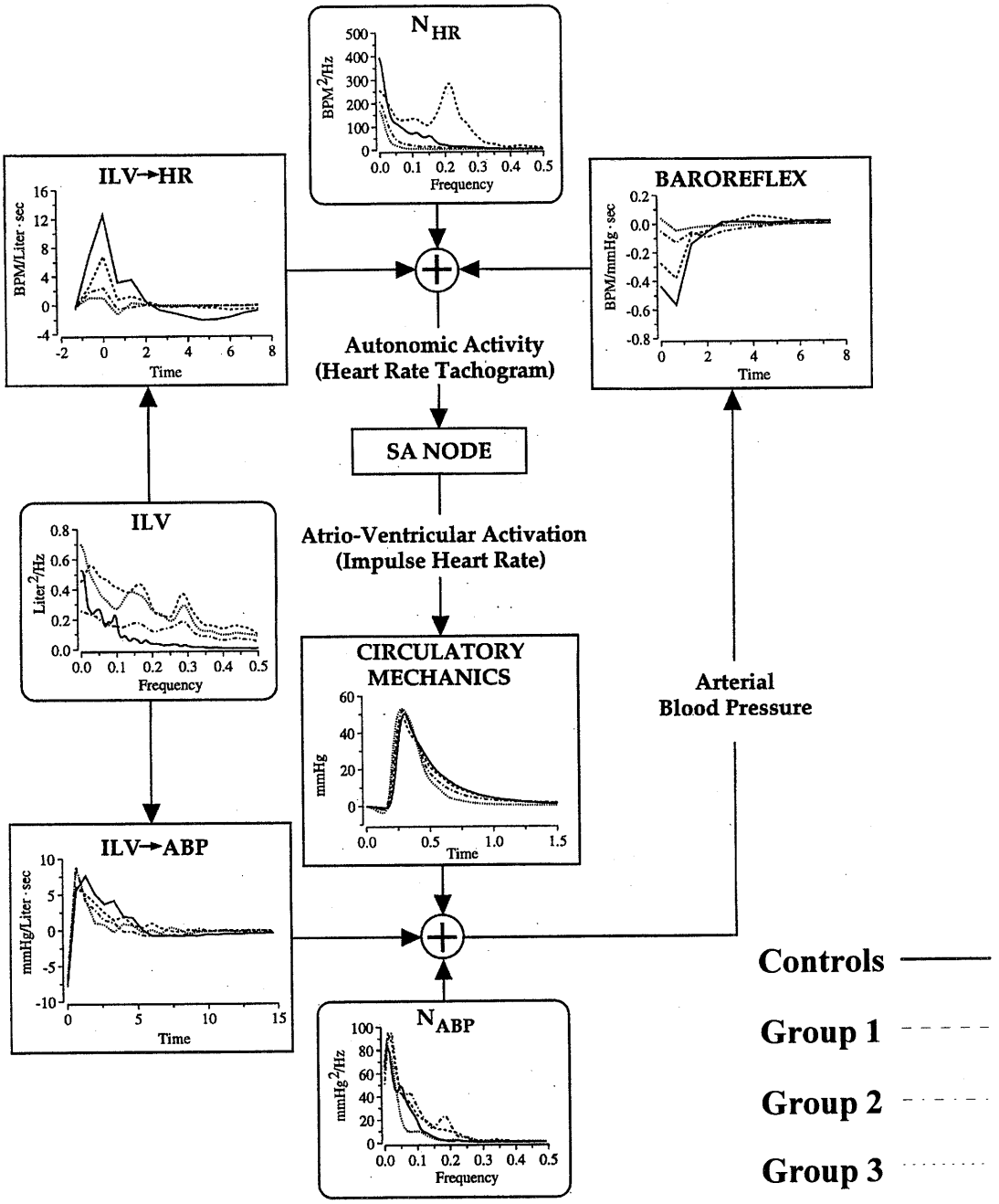

Figure 4-2: The averages of the closed-loop model estimates for the diagnostic groups in the supine posture.

Table 4-1: ANOVA and Multiple Comparison test results for the ILV→HR parameters.

ILV→HR Parameter	Mean±SEM Controls	Group 1	Group 2	Group 3	ANOVA p-value	Significant Multiple Comparisons
supine peak amplitude [ln(BPM/Liter-sec)]	2.35±0.14	1.60±0.21	1.33±0.19	0.98±0.09	<0.000005	$C1^{a}$; $C2^{b}$; $C3^{c}$
supine area [BPM/Liter]	4.52±5.61	1.49±3.38	0.85±3.34	0.55±2.34	NS	--
supine characteristic time [ln(sec)]	1.18±0.12	1.55±0.19	1.65±0.31	1.46±0.20	NS	--
tilted peak amplitude [ln(BPM/Liter-sec)]	1.95±0.11	1.43±0.16	1.17±0.11	0.83±0.13	<0.000005	$C1^{a}$; $C2^{a}$; $C3^{c}$; 13^{a}
tilted area [BPM/Liter]	3.28±3.52	-2.94±2.34	-1.76±2.41	-2.27±1.13	NS	--
tilted characteristic time [ln(sec)]	1.57±0.16	1.56±0.19	1.47±0.41	1.90±0.26	NS	--

C, control; 1, Group 1; 2, Group 2; 3, Group 3; a, p<0.0005; b, p<0.005; c, p<0.05; NS, not significant. $C1^{a}$ denotes that the mean of the control group is significantly different from the mean of Group 1 with a p-value <0.0005. The other Multiple Comparison results follow accordingly.

Table 4-2: ANOVA and Multiple Comparison test results for the BAROREFLEX parameters.*

BAROREFLEX Parameter	Mean±SEM Controls	Group 1	Group 2	Group 3	ANOVA p-value	Significant Multiple Comparisons
supine peak amplitude [ln(BPM/mmHg-sec)]	0.43±0.05	0.32±0.07	0.16±0.04	0.05±0.02	<0.00005	$C2^{a}$; $C3^{b}$; 13^{a}
supine area [BPM/mmHg]	-0.54±0.13	-0.23±0.07	-0.28±0.14	-0.12±0.06	NS	--
supine characteristic time [ln(sec)]	1.35±0.08	1.48±0.16	1.67±0.25	2.12±0.36	<0.05	none
tilted peak amplitude [ln(BPM/mmHg-sec)]	0.32±0.04	0.23±0.04	0.15±0.03	0.07±0.02	<0.0005	$C2^{a}$; $C3^{c}$; 13^{a}
tilted area [BPM/mmHg]	-1.00±0.18	-0.66±0.17	-0.58±0.17	-0.17±0.09	<0.05	$C3^{a}$
tilted characteristic time [ln(sec)]	1.75±0.13	1.89±0.14	1.89±0.29	2.36±0.21	NS	--

**See Table 4-1 for abbreviations.*

Table 4-3: ANOVA and Multiple Comparison test results for the ILV→ABP parameters.*

ILV→ABP Parameter	Mean±SEM Controls	Group 1	Group 2	Group 3	ANOVA p-value	Significant Multiple Comparisons
supine peak amplitude [ln(mmHg/Liter-sec)]	2.30±0.12	2.08±0.14	2.11±0.22	2.19±0.16	NS	--
supine area [mmHg/Liter]	8.64±8.32	11.08±4.02	-0.80±15.14	2.87±8.95	NS	--
supine characteristic time [ln(sec)]	1.75±0.10	1.66±0.12	1.69±0.20	1.98±0.18	NS	--
tilted peak amplitude [ln(mmHg/Liter-sec)]	2.21±0.07	2.00±0.12	2.09±0.17	2.02±0.11	NS	--
tilted area [mmHg/Liter]	6.47±2.59	4.38±2.47	11.35±5.68	15.10±7.16	NS	--
tilted characteristic time [ln(sec)]	1.80±0.09	1.78±0.08	1.57±0.10	1.84±0.14	NS	--

**See Table 4-1 for abbreviations.*

Table 4-4: ANOVA and Multiple Comparison test results for the CIRCULATORY MECHANICS parameters.*

CIRCULATORY MECHANICS Parameter	Mean±SEM Controls	Group 1	Group 2	Group 3	ANOVA p-value	Significant Multiple Comparisons
supine peak amplitude [ln(mmHg)]	4.01±0.04	3.96±0.07	4.00±0.09	4.05±0.08	NS	--
supine area [mmHg-sec]	17.34±1.19	17.10±1.75	18.74±4.20	13.43±1.44	NS	--
supine characteristic time [ln(sec)]	-0.70±0.04	-0.72±0.06	-0.78±0.13	-1.01±0.04	<0.05	$C3^{a}$; 13^{a}
tilted peak amplitude [ln(mmHg)]	3.74±0.04	3.82±0.07	3.83±0.10	3.65±0.11	NS	--
tilted area [mmHg-sec]	11.60±0.76	12.95±1.27	14.47±2.69	10.40±1.21	NS	--
tilted characteristic time [ln(sec)]	-0.71±0.03	-0.70±0.07	-0.71±0.10	-0.79±0.05	NS	--

**See Table 4-1 for abbreviations.*

Table 4-5: ANOVA and Multiple Comparison test results for the N_{HR} parameters.*

N_{HR} Parameter	Mean±SEM Controls	Group 1	Group 2	Group 3	ANOVA p-value	Significant Multiple Comparisons
supine total power [ln(BPM^2)]	2.47±0.18	1.99±0.32	1.33±0.25	0.05±0.38	<0.000005	$C3^{c}$; 12^{a}; 13^{b}
supine LF power [ln(BPM^2)]	2.37±0.18	1.90±0.31	1.24±0.25	-0.03±0.40	<0.000005	$C3^{c}$; 13^{b}
supine HF power [ln(BPM^2)]	-0.12±0.20	-0.83±0.37	-1.75±0.32	-2.89±0.24	<0.0000005	$C2^{a}$; $C3^{c}$; 13^{b}
tilted total power [ln(BPM^2)]	2.60±0.17	2.20±0.26	1.54±0.28	0.26±0.23	=0.0000000	$C2^{a}$; $C3^{c}$; 12^{a}; 13^{c}
tilted LF power [ln(BPM^2)]	2.55±0.17	2.14±0.25	1.46±0.29	0.12±0.26	=0.0000000	$C2^{a}$; $C3^{c}$; 12^{a}; 13^{c}
tilted HF power [ln(BPM^2)]	-0.55±0.23	-0.99±0.33	-1.64±0.36	-2.80±0.27	<0.00005	$C3^{c}$; 13^{b}

**See Table 4-1 for abbreviations.*

Table 4-6: ANOVA and Multiple Comparison test results for the N_{ABP} parameters.*

N_{ABP} Parameter	Mean±SEM Controls	Group 1	Group 2	Group 3	ANOVA p-value	Significant Multiple Comparisons
supine total power [ln($mmHg^2$)]	1.03±0.14	1.19±0.15	0.92±0.28	0.45±0.23	NS	--
supine LF power [ln($mmHg^2$)]	0.91±0.15	1.08±015	0.80±0.30	0.30±0.25	NS	--
supine HF power [ln($mmHg^2$)]	-1.53±0.13	-1.54±0.25	-1.59±0.24	-1.89±0.28	NS	--
tilted total power [ln($mmHg^2$)]	1.63±0.11	1.64±0.14	1.47±0.17	0.94±0.18	<0.05	$C3^{a}$; 13^{a}
tilted LF power [ln($mmHg^2$)]	1.56±0.12	1.59±0.14	1.40±0.18	0.82±0.18	<0.005	$C3^{a}$; 13^{a}
tilted HF power [ln($mmHg^2$)]	-1.52±0.15	-1.58±0.16	-1.37±0.25	-1.67±0.25	NS	--

**See Table 4-1 for abbreviations.*

Table 4-7: ANOVA test results for a sample by sample comparison among the impulse responses of the diagnostic groups

Impulse Response	Significant Differences (α<0.05)
supine ILV->HR	yes
tilted ILV->HR	yes
supine BAROREFLEX	yes
tilted BAROREFLEX	yes
supine ILV->ABP	no
tilted ILV->ABP	no
supine CIRCULATORY MECHANICS	yes
tilted CIRCULATORY MECHANICS	no

Yes indicates that the impulse response is significantly different for at least one sample across the diagnostic groups. No indicates that all the samples of the impulse response are statistically the same across the diagnostic groups.

Table 4-8: ANOVA test results for a sample by sample comparison among the noise spectra of the diagnostic groups

Noise Spectra (ln)	Significant Differences (α<0.05)
supine NHR	yes
tilted NHR	yes
supine NABP	no
tilted NABP	no

Yes indicates that the noise spectra is significantly different for at least one sample across the diagnostic groups. No indicates that all the samples of the noise spectra are statistically the same across the diagnostic groups.

contraction. The power spectrum of the noise perturbation N_{HR} is about the same for the Control group and Group 1 but then diminishes across the remaining diabetic groups as autonomic neuropathy progresses. These power spectra show that fluctuations in ILV and ABP do not completely account for HR fluctuations less than 0.1 Hz. The power spectrum of the noise perturbation N_{ABP} is roughly the same for the Control group, Group 1, and Group 2 but is diminished for Group 3. These power spectra show that

fluctuations in ILV and IHR do not explain all the ABP variability less than 0.2 Hz. Finally, note that the power spectrum for ILV appears to be broadband with significant spectral content within 0.5 Hz for all the diagnostic groups. Figure 4-2 shows that similar averages result from data collected while the subjects were in the supine posture.

The results of the ANOVA and multiple comparison tests comparing each parameter of the impulse response and noise perturbation estimates across the diagnostic groups are shown in Tables 4-1 through 4-6. As mentioned in Section 4.1.3, the impulse response and noise perturbation estimates were characterized with three parameters each. The impulse responses and noise perturbations are estimated for data collected while the subjects were in both the supine and tilted postures, so six parameters are presented in each table.

Table 4-1 shows the ILV→HR parameter comparison results. Both mean supine peak amplitude and mean tilted peak amplitude are significantly different across the diagnostic groups with the mean being largest for the Control group and then decreasing with the progressing autonomic neuropathy of the diabetic groups. For each of these parameters, the Control group mean is significantly larger than those of the three diabetic groups. Additionally, the Group 1 mean of tilted peak amplitude is significantly larger than that of Group 3. The other four parameters involving area and characteristic time did not provide any significant differences across the diagnostic groups.

Table 4-2 shows the BAROREFLEX parameter comparison results. Both mean supine peak amplitude and mean tilted peak amplitude are significantly different across the diagnostic groups with the mean being largest for the Control group and then decreasing with the progressing autonomic neuropathy of the diabetic groups. For each of these parameters, the Control group mean is significantly larger than those of Group 2 and Group 3, and the Group 1 mean is significantly larger than that of Group 3. The mean of supine characteristic time is also significantly different across the diagnostic groups with the mean being smallest for the Control group and then increasing as the autonomic neuropathy of the diabetic groups progresses. However, there are no significant differences between any two particular groups. Additionally, the mean of

tilted area is significantly different across the diagnostic groups with a trend in the means similar to that of supine characteristic time. The Control group mean for tilted area is significantly smaller than that of Group 3. There are no significant differences resulting from the remaining two parameters of supine area and tilted characteristic time across the diagnostic groups.

Table 4-3 shows the ILV→ABP parameter comparison results. There are no significant differences resulting from any of the six parameters across the diagnostic groups.

Table 4-4 shows the CIRCULATORY MECHANICS parameter comparison results. The mean of the supine characteristic time is significantly different across the diagnostic groups with the mean being largest for the Control group and then decreasing with the progressing autonomic neuropathy of the diabetic groups. For this parameter, the Control group mean and the Group 1 mean are significantly smaller than that of Group 3. The other five parameters provide no significant differences across the diagnostic groups.

Table 4-5 shows the N_{HR} parameter comparison results. The mean of all six parameters are significantly different across the diagnostic groups with the mean being largest for the Control group and then decreasing as the autonomic neuropathy of the diabetic groups progresses. There are many significant differences between pairs of the four groups mostly involving differences between the Control group or Group 1 and Group 2 or Group 3.

Table 4-6 shows the N_{ABP} parameter comparison results. The mean of the tilted total power and tilted low frequency power are significantly different across the diagnostic groups with the mean being about the same for the Control group and Group 1 and then decreasing with the progressing autonomic neuropathy of the remaining diabetic groups. For each of these parameters, the Control group mean and Group 1 mean are significantly larger than that of Group 3.

The results of the ANOVA tests comparing the impulse response and noise perturbation estimates nonparametrically across the diagnostic groups are respectively

shown in Tables 4-7 and 4-8. The results are shown for estimates obtained from data collected while the subjects were in both the supine and tilted postures. These results matched well with the parametric comparison. For every estimate found to be significantly different across the diagnostic groups by the nonparametric comparison, at least one parameter associated with that estimate was also found to be significantly different across the diagnostic groups. The converse of this statement also holds with the one exception being tilted N_{ABP}.

4.3 Discussion

The results of this study support the role of closed-loop system identification in the assessment of autonomic nerve damage in patients with diabetes mellitus. There were marked differences in the ILV→HR and BAROREFLEX impulse responses and minor differences in the CIRCULATORY MECHANICS impulse response across the diagnostic groups. These results were expected as the ILV→HR and BAROREFLEX impulse responses are autonomically mediated, whereas the CIRCULATORY MECHANICS impulse response is primarily mediated by mechanical mechanisms but is also sympathetically influenced. Additionally, there were no significant differences in the ILV→ABP impulse responses across the diagnostic groups. This was also expected as the ILV→ABP impulse response is mechanical mediated and dysfunction of mechanical mechanisms is not assumed to be associated with diabetic autonomic neuropathy.

The parameters used to characterize the impulse response and noise perturbation estimates provided statistically significant differences across the diagnostic groups only for the impulse responses and noise perturbations that are autonomically influenced. Specifically, the peak amplitude parameter provided significant differences across the diagnostic groups for the ILV→HR and BAROREFLEX impulse responses; the area parameter provided significant differences across the diagnostic groups for the tilted BAROREFLEX impulse response; and the characteristic time parameter provided significant differences across the diagnostic groups for the supine BAROREFLEX

impulse response. These significant differences showed that the mean peak amplitude and absolute area are largest for the Control group and decrease with the progressing autonomic neuropathy of the diabetic groups. The significant differences also showed that the mean characteristic time is smallest for the Control group and increases with the progressing autonomic neuropathy of the diabetic groups. Decreasing peak amplitude and absolute area reflect attenuation in the impulse response, while increasing characteristic time reflects sluggishness in the impulse response. The peak amplitude is clearly the most reliable discriminant parameter. Additionally, the BAROREFLEX seems to be more sensitive to the parameters of the impulse response estimates than ILV→HR which further emphasizes closed-loop system identification.

The characteristic time parameter provided a significant difference across the diagnostic groups for the supine CIRCULATORY MECHANICS impulse response with the characteristic time being largest for the Control group and then decreasing with the progressing autonomic neuropathy of the diabetic groups. However, this parameter was practically the same in all the diagnostic groups excluding Group 3 which was much smaller than the other three groups. The decrease in characteristic time essentially corresponds to a decrease in peripheral vascular resistance. Therefore, this may indicate that damage of the α sympathetic pathways which are responsible for vasoconstriction occurs late in the natural history of diabetic autonomic neuropathy. This result is supported by findings from the standard autonomic tests [16]. However, these findings could also have been due to the insensitivity of these tests in detecting early sympathetic nerve damage.

All the parameters derived from the noise perturbation N_{HR} provided significant differences across the diagnostic groups with the mean being largest for the Control group and then decreasing with the progressing autonomic neuropathy of the diabetic groups. This seems reasonable as HR is almost exclusively modulated by autonomic mechanisms. On the other hand, the parameters for the noise perturbation N_{ABP} provided significant differences only for the tilted posture. However, this was not supported by the

nonparametric comparison which found no significant differences across the diagnostic groups for tilted N_{ABP}.

The results of the parametric and nonparametric comparisons matched almost identically with the exception of tilted N_{ABP}. Therefore, the nonparametric comparison which is a "brute force" method to compare impulse response and noise perturbation estimates supports the choice of parameters. These parameters provide a much more intuitive approach to comparing these estimates.

By definition, the mean A score of the Control group is zero. According to the tests used to rank the diabetic subjects, Group 1 diabetics somewhat better autonomic function than the control subjects. However, the results of closed-loop system identification illustrate quite the contrary i.e., the control subjects have better autonomic function than Group 1 diabetics. This indicates the greater sensitivity of the closed-loop system identification over the currently accepted tests that were used to rank the diabetic subjects.

4.4 Conclusion

In this chapter and the previous chapter, a new test for the assessment of the autonomic nerve damage associated with diabetes mellitus was introduced. As with the introduction of any new test, a comparison with the currently accepted tests is required. This study shows that marked differences in the two autonomically mediated impulse response estimates (ILV→HR and BAROREFLEX) and minor differences in the impulse response estimate that is primarily mechanically mediated but also autonomically influenced (CIRCULATORY MECHANICS) were found across the diagnostic groups defined by the current accepted tests. Just as important, significant differences were not found in the mechanically mediated impulse response estimates (ILV→ABP) across these diagnostic groups. Although the results were presented as group averages, it is essential to realize that closed-loop system identification was applied here to individuals and not groups. Consequently, the application of this method results in a personal description of the status of the short-term cardiovascular control mechanisms of a particular individual.

Therefore, closed-loop system identification may provide a sensitive, quantitative, and noninvasive method that requires minimal subject cooperation for the assessment of diabetic autonomic neuropathy.

Chapter 5

Nonlinear System Identification Applied to Normal Heart Rate Variability

In this thesis, the couplings between the small beat-to-beat fluctuations in cardiovascular signals about their mean values that result from stable experimental conditions are assumed be related linearly. However, previous experimental work has shown that the full repertoire of these couplings also includes nonlinear dynamics, specifically those couplings involving HR as the output [29,42]. This chapter presents a preliminary investigation of the nonlinear dynamics involved in the generation of HR variability. In particular, the significance of the squared and cross product terms of ABP and ILV on HR is explored using input-output data from control subjects.

5.1 Complexity of Nonlinear System Identification

Nonlinear analysis is typically avoided in most engineering problems due to its extreme complexities. Consequently, unlike linear analysis, nonlinear analysis is a field that is still developing. However, some nonlinear problems can be solved using linear analysis. System identification involving the estimation of nonlinear models is one example of this. A nonlinear description of a dynamic system can be viewed in some

cases as a linear mapping of an infinite number of inputs to an output. Consider a system with inputs $u_1(t)$ and $u_2(t)$ and output $y(t)$, a nonlinear description of this system might then be represented as follows:

$$y(t) = L\{u_1(t), u_2(t), u_1^2(t), u_2^2(t), u_1(t)u_2(t), u_1^3(t), u_2^3(t), u_1^2(t)u_2(t), \ldots\}$$

where $L\{\}$ is a linear transformation that maps inputs to a output. Note that this equation is similar to a Taylor series expansion of analytic functions. This concept also can be extended to an ARMA linear constant coefficient difference equation (LCCDE) as follows:

$$y(t) = \sum_{k=1}^{A} b_{1k} y(t-k) + \sum_{k=B'}^{B} b_{2k} u_1(t-k) + \sum_{k=C'}^{C} b_{3k} u_2(t-k) + \sum_{k=D'}^{D}\sum_{j=E'}^{E} b_{1kj} u_1(t-k)u_1(t-j) +$$

$$\sum_{k=F'}^{F}\sum_{j=G'}^{G} b_{2kj} u_2(t-k)u_2(t-j) + \sum_{k=1}^{I}\sum_{j=1}^{J} b_{3kj} y(t-k)y(t-j) + \sum_{k=K'}^{K}\sum_{j=L'}^{L} b_{4kj} u_1(t-k)u_2(t-j) + \cdots$$

Note that this equation is further complicated because the output and lags additionally play a role in the nonlinear terms. In this equation, there are nonlinear terms, but these terms can be created as products of the linear terms. Therefore, the equation remains linear in its parameters and so, LTI analysis applies here. However, LTI analysis does not make the problem any less complicated, since identifying the parameters of such an equation is an impossible task. Even system identification involving only the second order nonlinear terms in this equation is a difficult problem and could be a thesis in its own right. However, system identification involving a few nonlinear terms is quite manageable and so, the objective of this chapter is to provide a simple, preliminary nonlinear analysis.

5.2 Nonlinear System Identification Procedure

Although the first step in the general system identification procedure is to generate the input-output data, the selection of the candidate set of models is presented first for convenience. It seems reasonable to select the form of the candidate difference equation by simply introducing second order nonlinear terms to the ARMA difference equation in (3.15) as follows:

$$HR(t) = \sum_{k=1}^{Q} a_k HR(t-k) + \sum_{k=1}^{R} d_{1k} ABP(t-k) + \sum_{k=S'}^{S} d_{2k} ILV(t-k) + \tag{5.1}$$

$$\sum_{k=1}^{R} d_{3k} ABP^2(t-k) + \sum_{k=S'}^{S} d_{4k} ILV^2(t-k) + \sum_{k=1}^{R} d_{5k} ABP(t-k) ILV(t-k) + W_{HR}(t)$$

where $W_{HR}(t)$ is again the residual error and is defined to be a white, Gaussian noise process. The particular nonlinear terms $ABP^2(t)$, $ILV^2(t)$, and $ABP(t)ILV(t)$ are included in this equation as opposed to nonlinear terms with non-zero lag, because they seem more likely to influence $HR(t)$. The squared and cross product terms of $HR(t)$ also seem likely to influence $HR(t)$; however, the inclusion of such terms in (5.1) resulted in unstable models.

The HR, ABP, and ILV data necessary for the estimation of the parameters in (5.1) is generated as discussed in Section 3.1 except that this time the data is decimated to 3 Hz as opposed to 1.5 Hz. The nonlinear terms are viewed simply as separate inputs and are created from the ABP and ILV data accordingly. The input-output data which now consists of six signals are then divided into two equal length segments. The rationale for this will be discussed in the next section. The "best" model was determined with the method in Section 3.4 using only the first half of the input-output data segment. Therefore, since the data is sampled at 3 Hz, the same number of data samples are used in this estimation procedure and the closed-loop system identification procedure. It should be noted that this estimation procedure may lead to inconsistent estimates even if the form and order of this difference equation matches the dynamics of the true system. In particular, the covariance matrix $E(\phi(t)\phi^{\mathrm{T}}(t))$ might be singular. The resulting nonlinear model estimates are validated again with residual error analysis since whiteness is a requirement of the residual errors. But validation based on *a priori* information is difficult in this case as the couplings between the nonlinear terms and HR are poorly understood. This nonlinear system identification procedure was applied to the input-output data from each of the 37 control subjects introduced in Section 4.1.1.

5.3 Comparison with Linear System Identification

The significance of the three nonlinear terms in the generation of HR variability was assessed by comparing the predictive value of the estimated nonlinear model with that of an estimated linear model for each subject. The linear model was estimated in the same manner as the nonlinear model except the form of the candidate set of models was that in (3.15). The predictive value of each estimated model was determined by calculating the NMSE for the predicted $\{HR(t)\}$ sequence as follows:

$$NMSE = \frac{Var(HR_{actual}(t) - HR_{predicted}(t))}{Var(HR_{actual}(t))}.$$

The predicted $\{HR(t)\}$ sequence is determined by computing each value of the $\{HR(t)\}$ sequence from the estimated model, the actual past values of the $\{HR(t)\}$ sequence, and the actual values of the inputs. In determining the predictive value of the estimated models, the second half of the input-output data segment is used. Therefore, the first half of the data was used to "learn" about the dynamic system and the second half of the data was used to "predict" the output based on what had been already learned. The division of the input-output data into two segments is essential here. The estimated nonlinear model will generally contain more parameters than that of the estimated linear model. This will typically result in a lower NMSE for the estimated nonlinear model when the data used for prediction is the same as that used for learning. However, when the data used for prediction is different from that used for learning, the number of parameters is no longer a factor. Table 5.1 shows the NMSE's resulting from the estimated linear and nonlinear models for each control subject in both the supine and tilted postures. The mean NMSE's resulting from the estimated linear and nonlinear models are calculated and compared via paired t tests. Table 5.2 shows the results of these t tests for data collected while the subjects were in both the supine and tilted postures. These results show that the nonlinear terms do not significantly influence HR variability in either the supine or tilted posture, because the mean NMSE's resulting from both estimated models are the same for each posture.

Table 5-1: NMSE of predicted HR from estimated linear and nonlinear models for each control subject in both supine and tilted postures.

Subjects	Supine Posture		Tilted Posture	
	Linear NMSE	Nonlinear NMSE	Linear NMSE	Nonlinear NMSE
subject #1	0.045146	0.047326	0.014398	0.014051
subject #2	0.034232	0.040499	0.008705	0.008326
subject #3	0.0197	0.016916	0.04908	0.057132
subject #4	0.031648	0.029393	0.012862	0.017846
subject #5	0.035504	0.040245	0.01757	0.017177
subject #6	0.018636	0.019295	0.012854	0.014929
subject #7	0.022278	0.027094	0.018778	0.015585
subject #8	0.033729	0.031555	0.01113	0.01172
subject #9	0.02363	0.024859	0.030869	0.030965
subject #10	0.062514	0.067789	0.017397	0.013394
subject #11	0.043625	0.057698	0.008311	0.008553
subject #12	0.035898	0.038212	0.014166	0.015884
subject #13	0.038241	0.04046	0.069628	0.070025
subject #14	0.035841	0.036966	0.050967	0.052357
subject #15	0.032306	0.032741	0.018556	0.017012
subject #16	0.044911	0.051931	0.020399	0.03109
subject #17	0.015362	0.014929	0.012605	0.010518
subject #18	0.031027	0.026391	0.027997	0.024245
subject #19	0.035034	0.036853	0.007026	0.008322
subject #20	0.036024	0.036527	0.024742	0.02349
subject #21	0.02911	0.025092	0.020022	0.021879
subject #22	0.065946	0.071654	0.024732	0.02404
subject #23	0.04055	0.041697	0.187177	0.187177
subject #24	0.032093	0.032696	0.076432	0.072555
subject #25	0.028997	0.030163	0.017158	0.019405
subject #26	0.082688	0.082174	0.141445	0.154633
subject #27	0.028649	0.025703	0.015374	0.015877
subject #28	0.021902	0.015263	0.02489	0.022754
subject #29	0.063156	0.070411	0.037139	0.037802
subject #30	0.028569	0.032832	0.005126	0.004491
subject #31	0.023491	0.032763	0.008789	0.007565
subject #32	0.012399	0.017906	0.008457	0.008524
subject #33	0.017256	0.019341	0.014424	0.013267
subject #34	0.047969	0.04181	0.022536	0.020319
subject #35	0.059446	0.026127	0.007058	0.007409
subject #36	0.028391	0.02761	0.010721	0.010184
subject #37	0.059419	0.060959	0.010818	0.01165

Table 5.2: T test results comparing the mean NMSE of predicted HR from estimated linear models and the mean NMSE of predicted HR from estimated nonlinear models.

	Mean ± SEM		
Posture	Linear NMSE	Nonlinear NMSE	p-value
supine	0.036 ± 0.003	0.037 ± 0.003	NS
tilted	0.029 ± 0.006	0.030 ± 0.006	NS

Although the results of this comparison show that $ABP^2(t)$, $ILV^2(t)$, and $ABP(t)ILV(t)$ do not influence $HR(t)$, this by no means indicates that nonlinear dynamics do not play a role in the generation of HR variability. These terms might not have been significant because the nonlinear system identification procedure may have resulted in inconsistent estimates. On the other hand, the estimates could be consistent and these particular nonlinear terms just do not influence HR. This nonlinear system identification procedure was implemented as a preliminary analysis of the nonlinear dynamics involved in the generation of HR. Although the treatment of this procedure was not nearly as rigorous as the closed-loop system identification procedure in Chapter 3, this nonlinear analysis emphasizes the necessity for a more complete study of the nonlinear dynamics involved in the generation of HR and short-term cardiovascular control in general. However, the preliminary conclusion from this analysis is that the linear terms probably dominate in the generation of HR variability under stable experimental conditions. Therefore, this analysis supports the focus of the closed-loop system identification procedure on linear terms.

Bibliography

[1] Akselrod S., D. Gordon, F.A. Ubel, D.C. Shannon, A.C. Barger, and R.J. Cohen. *Power Spectrum Analysis of Heart Rate Fluctuations: A Quantitative Probe of Beat-to-Beat Cardiovascular Control.* ***Science,*** 213, 220-222, 1981.

[2] Appel M.L. ***Closed Loop Identification of Cardiovascular Regulatory Mechanisms.*** Ph.D. Thesis, The Division of Applied Sciences, Harvard University, 1992.

[3] Appel M.L., R.D. Berger, J.P. Saul, J.M. Smith, and R.J. Cohen. *Beat to Beat Variability in Cardiovascular Variables: Noise or Music?* ***Journal of the American College of Cardiology***, 14, 1139-1148, 1989.

[4] Appel M.L., T.J. Mullen, J.M. Mathias, R. Mukkamala, M.H. Perrot, J.P. Saul, and R.J. Cohen: *System Identification of Closed-Loop Cardiovascular Control Mechanisms: I - Autonomic Pharmacological Blockade.* Ms in Prep.

[5] Astrom K.J. and P. Eykhoff. *System Identification - A Survey.* ***Automatica***, 7, 123-162, 1971.

[6] Baselli G., S. Cerutti, S. Civardi, A. Malliani, and M. Pagani. *Cardiovascular Variability Signals: Towards the Identification of a Closed-Loop Model of the Neural Control Mechanisms.* ***IEEE Transactions on Biomedical Engineering***, BME-35, 1033-1046, 1988.

[7] Bellavere F., I. Balzani, G. De Masi, M. Carraro, P. Carenza, C. Cobelli, and K. Thomaseth. *Power Spectral Analysis of Heart-Rate Variations Improves Assessment of Diabetic Cardiac Autonomic Neuropathy.* ***Diabetes***, 41, 633-640, 1992.

[8] Berger R.D. ***Analysis of the Cardiovascular Control System Using Broad-Band Stimulation***. Ph.D. Thesis, Department of Electrical Engineering and Computer Science, Massachusetts Institute of Technology, 1987.

[9] Berger R.D., J.P. Saul, and R.J. Cohen. *Assessment of Autonomic Response by Broad-Band Respiration.* ***IEEE Transactions on Biomedical Engineering***, 36, 1061-1065, 1989.

[10] Berger R.D., J.P. Saul, and R.J. Cohen. *Transfer Function Analysis of Autonomic Regulation: I - The Canine Atrial Rate Response.* ***American Journal of Physiology - Heart and Circulatory Physiology***, 25, H142-152, 1989.

[11] Berger R.D., S. Akselrod, D. Gordon, and R.J. Cohen. *An Efficient Algorithm for Spectral Analysis of Heart Rate Variability.* ***IEEE Transactions on Biomedical Engineering***, 33, 900-904, 1986.

[12] Caro C.G., T.J. Pedley, R.C. Schroter, and W.A. Seed. ***The Mechanics of the Circulation***. Oxford University Press, New York, NY, 1978.

[13] Clarke B.F., D.J. Ewing, and I.W. Campbell. *Diabetic Autonomic Neuropathy.* ***Diabetologia***, 17, 195-212, 1979.

[14] Cohen R.J. *Hemodynamics I, II, III.* Not Published.

[15] Ewing D.J. and B.F. Clarke. *Diabetic Autonomic Neuropathy: Present Insight and Future Prospects.* ***Diabetes Care***, 9, 648-655, 1986.

[16] Ewing D.J., C.N. Martyn, R.J. Young, and B.F. Clarke. *The Value of Cardiovascular Autonomic Function Tests: 10 Years Experience in Diabetes.* ***Diabetes Care***, 8, 491-498, 1985.

[17] Ewing D.J., I.W. Campbell, and B.F. Clarke. *Mortality in Diabetic Autonomic Neuropathy.* ***Lancet***, I, 601-603, 1976.

[18] Fisher L.D. and G. Van Belle. ***Biostatistics: A Methodology for the Health Sciences***. John Wiley & Sons, Inc., New York, NY, 1993.

[19] Freeman R. *Testing the Autonomic Nervous System.* Not Published.

[20] Freeman R., J.P. Saul, M.S. Roberts, R.D. Berger, C. Broadbridge, and R.J. Cohen. *Spectral Analysis of Heart Rate in Diabetic Autonomic Neuropathy.* ***Archives of Neurology***, 48, 185-190, 1991.

[21] Freeman R., R.J. Cohen, and J.P. Saul. *Transfer Function Analysis of Respiratory Sinus Arrhythmia: A Measure of Autonomic Function in Diabetic Neuropathy.* ***Muscle and Nerve***, 18, 74-84, 1995.

[22] Ganong W.F. ***Review of Medical Physiology***. Appleton & Lange, Norwalk, CT, 1987.

[23] Guyton A.C. ***Textbook of Medical Physiology***. W.B. Saunders Co., Philadelphia, PA, 1981.

[24] Hsia T.C. ***System Identification: Least-Squares Methods***. D.C. Heath and Co., Lexington, MA, 1977.

[25] Hyndman B.W. and R.K. Mohn. *A Pulse Modulator Model for Pacemaker Activity.* ***Dig. 10th Int. Conf. Med. Biol. Eng.***, 223, 1973.

[26] Kenet R.O. ***Closed-Loop Identification of Hemodynamic Control***. Ph.D. Thesis, Department of Electrical Engineering, Yale University, 1983.

[27] Lishner M., S. Akselrod, V. Mor Avi, O. Oz, M. Divon, and M. Ravid. *Spectral Analysis of Heart Rate Fluctuations. A Non-Invasive, Sensitive Method for the Early Diagnosis of Autonomic Neuropathy in Diabetes Mellitus.* ***Journal of the Autonomic Nervous System***, 19, 119-125, 1987.

[28] Ljung L. ***System Identification: Theory for the User***. Prentice-Hall, Inc., Englewood Cliffs, NJ, 1987.

[29] Mancia G. and A.L. Mark. *Arterial Baroreflexes in Humans* from ***Handbook of Physiology, Section 2: The Cardiovascular System, Vol. III***. American Physiological Society, Bethesda, MD, 1983.

[30] Marple L.S. ***Digital Spectral Analysis***. Prentice-Hall, Inc., Englewood Cliffs, NJ, 1987.

[31] Mathias J.M., T.J. Mullen, M.H. Perrott, and R.J. Cohen. *Heart Rate Variability: Principles and Measurement.* ***ACC Current Journal Review***, November/December 1993, 10-12.

[32] Oppenheim A.V. and R.W. Schafer. ***Discrete-Time Signal Processing***. Prentice-Hall, Inc., Englewood Cliffs, NJ, 1989.

[33] Pagani M., G. Malfatto, S. Pierini, R. Casati, A.M. Masu, M. Poli, S. Guzzetti, F. Lombardi, S. Cerutti, and A. Malliani. *Spectral Analysis of Heart Rate Variability in the Assessment of Autonomic Diabetic Neuropathy.* ***Journal of the Autonomic Nervous System***, 23, 143-153, 1988.

[34] Perrott M.H. ***An Efficient ARX Model Selection Procedure Applied to Autonomic Heart Rate Variability***. SM Thesis, Department of Electrical Engineering and Computer Science, Massachusetts Institute of Technology, 1992.

[35] Saul J.P., R.D. Berger, M.H. Chen, and R.J. Cohen. *Transfer Function Analysis of Autonomic Regulation: II - Respiratory Sinus Arrhythmia.* ***American Journal of Physiology - Heart and Circulatory Physiology***, 25, H153-H161, 1989.

[36] Saul J.P., R.D. Berger, P. Albrecht, S.P. Stein, M.H. Chen, and R.J. Cohen. *Transfer Function Analysis of the Circulation: Unique Insights into Cardiovascular Regulation.* ***American Journal of Physiology***, 261, H1231-H1245, 1991.

[37] Saul J.P. and R.J. Cohen. *Respiratory Sinus Arrhythmia* from ***Vagal Control of the Heart: Experimental Basis and Clinical Implications***. Futura Publishing Co., Inc., Armonk, NY, 1994.

[38] Shanmugan K.S. and A.M. Breipohl. ***Random Signals: Detection, Estimation, and Data Analysis***. John Wiley & Sons, Inc., New York, NY, 1988.

[39] Soderstrom T. and P. Stoica. ***System Identification***. Prentice-Hall, Inc., Englewood Cliffs, NJ, 1989.

[40] Strang G. ***Linear Algebra and its Applications***. Academic Press, Inc., New York, NY, 1980.

[41] Sundkvist G., B. Lilja, and L.O. Almer. *Abnormal Diastolic Blood Pressure and Heart Rate Reactions to Tilting in Diabetes Mellitus.* ***Diabetologia***, 19, 433-438, 1980.

[42] Taher M.F., A.B.P. Cecchini, M.A. Allen, S.R. Gobran, R.C. Gorman, B.L. Guthrie, K.A. Lingenfelter, S.Y. Rabbany, P.M. Rolchigo, J. Melbin, and A. Noordergraaf. *Baroreceptor Responses Derived From a Fundamental Concept.* ***Annals of Biomedical Engineering***, 16, 429-443, 1988.

[43] Wellstead P.E. and J.M. Edmunds. *Least-Squares Identification of Closed-Loop Systems.* ***International Journal of Control***, 21, 689-699, 1975.

[44] Willsky A.S. and G.W. Wornell. *Estimation Theory*. Not Published.

[45] Yana K., J.P. Saul, R.D. Berger, M.H. Perrott, and R.J. Cohen. *A Time Domain Approach for the Fluctuation Analysis of Heart Rate Related to Instantaneous Lung Volume.* ***IEEE Transactions on Biomedical Engineering***, 40, 74-81, 1993.